

Phenomenological energy exchange of diatomic gases: Comparison of Pullin and Borgnakke-Larsen models in direct simulation Monte Carlo method

Hao Jin (金浩),^{1, a)} Sha Liu (刘沙),^{1, 2, 3, b)} Ningchao Ding (丁宁超),¹ Sirui Yang (杨思睿),¹ Huahua Cui (崔华华),⁴ Congshan Zhuo (卓丛山),^{1, 2, 3} and Chengwen Zhong (钟诚文)^{1, 2, 3}

¹⁾*School of Aeronautics, Northwestern Polytechnical University, Xi'an, Shaanxi 710072, China*

²⁾*Institute of Extreme Mechanics, Northwestern Polytechnical University, Xi'an, Shaanxi 710072, China*

³⁾*National Key Laboratory of Aircraft Configuration Design, Northwestern Polytechnical University, Xi'an, Shaanxi 710072, China*

⁴⁾*Dawning Information Industry Co., Ltd, Binhai High-tech Industrial Development Zone, Tianjin 300384, China*

(Dated: 10 February 2026)

In hypersonic rarefied flows, insufficient intermolecular collisions cause significant deviations between translational and rotational temperatures, leading to strong thermal nonequilibrium. This behavior differs markedly from continuum flows, where these temperatures are nearly identical and can be represented by a reduced translational-rotational temperature. The redistribution of energy among different modes substantially affects the flow-field structure and surface heating of hypersonic vehicles, making accurate modeling of energy exchange essential for rarefied flow simulations. For diatomic gases such as nitrogen and oxygen, the direct simulation Monte Carlo (DSMC) method commonly employs the Borgnakke-Larsen (BL) model to simulate translational-rotational energy exchange (relaxation) processes. Although widely used, the BL model lacks a rigorous theoretical foundation and assumes that only a fraction of collisions lead to rotational relaxation, limiting its physical realism. To address these shortcomings, Pullin introduced a kinetically consistent relaxation model into the gas kinetic theory. By employing the Beta function for energy partitioning, a concrete collision cross section that satisfies the detailed balance condition is constructed. In this study, a comparative investigation of the BL and Pullin models is performed within the DSMC framework, where both original and simplified equations are considered and parameterized by physical accommodated coefficient in the Beta function. A series of test cases—including zero-dimensional rotational relaxation of nitrogen, one-dimensional planar Couette flow and normal shock wave, two-dimensional hypersonic flow past a cylinder, and three-dimensional hypersonic flow around an X38-like vehicle—are performed to assess the accuracy and efficiency of these models. The results confirm the consistency between the Pullin and BL models. Owing to its rigorous theoretical foundation and accurate physical representation, the Pullin model is expected to provide substantial support for the extension of subsequent theoretical studies and numerical simulations. Moreover, in the highly rarefied flow regime (Knudsen number greater than 1, or altitudes above 100 km), the simplified Pullin model exhibits performance comparable to that of the BL model.

^{a)}jinhhao@mail.nwpu.edu.cn

^{b)}Corresponding author: shaliu@nwpu.edu.cn

I. INTRODUCTION

In hypersonic flows, diatomic gases (e.g., N₂ and O₂) undergo complex energy exchange processes associated with their internal degrees of freedom (DOFs), including rotational and vibrational modes. Under continuum conditions at moderate altitudes, collisions occur frequently enough that energy transfer among translational, rotational, and vibrational modes tends toward equipartition—particularly between translational and rotational modes—thereby maintaining an approximate local thermodynamic equilibrium¹. At higher altitudes, however, the mean free path increases and collisional energy transfer becomes significantly slower. As a result, the relaxation times of internal energy modes may become comparable to characteristic flow timescales, giving rise to thermodynamic nonequilibrium^{2–4}. In this rarefied regime, the redistribution of energy among different modes strongly influences the flowfield structure, surface heating, and overall aerothermodynamic performance of hypersonic vehicles. Accurate modeling of such energy exchange processes is therefore essential in rarefied hypersonic gas dynamics.

To capture thermodynamic nonequilibrium phenomena in rarefied flows, a variety of numerical methods have been developed for solving the Boltzmann equation, which are generally categorized into deterministic approaches^{5–7} and stochastic particle approaches^{8–11}. Among these methods, the direct simulation Monte Carlo (DSMC)^{8,12} method has become the most widely used stochastic approach for rarefied nonequilibrium gas flows. The DSMC method decouples molecular motion and collisions within each time step: molecules are first advanced in free transport at constant velocity, after which representative collision pairs are selected through probabilistic sampling. By explicitly modeling molecular collision pairs, the DSMC method can efficiently incorporate complex physico-chemical processes—including translational-internal energy exchange^{13,14}, chemical reactions^{15,16}, and ionization¹⁷—without significantly increasing the computational cost, making it particularly well suited for hypersonic nonequilibrium flow simulations.

Several phenomenological models^{18–23} for translational-internal energy exchange have been proposed and implemented in DSMC simulations. Among them, the Borgnakke-Larsen (BL) model¹⁸, proposed in 1975, is the most widely adopted approach for modeling energy transfer between translational and internal modes in diatomic molecules. In the BL model, a fraction of colliding particles is randomly selected to undergo inelastic collisions. Elastic

collisions involve only changes in particle velocities, while inelastic collisions redistribute post-collision energies between translational and internal modes, with the new energies sampled from an equilibrium distribution corresponding to the collision energy. The probability of inelastic collisions is determined by a relaxation collision number, which enables this model to reproduce experimentally observed relaxation rates²⁴. When the temperature-dependent relaxation models were introduced—such as Parker’s model for rotational energy²⁵ and the Millikan-White correlation for vibrational energy²⁶—it was shown that the detailed balance principle is satisfied if the probability of energy exchange depends exclusively on collision invariants (total collisional energy)¹⁴. The BL model is simple and computationally efficient; however, it is physically unrealistic, as only a fraction of collisions are inelastic. To improve its physical fidelity, a restricted energy exchange⁸ variant of the model has been proposed, in which all colliding particles undergo inelastic collisions. However, this modification compromises computational efficiency and has been shown not to satisfy the detailed balance principle^{8,19}. During energy exchange, the principle of detailed balance requires that, at equilibrium, the probability of a forward collision must equal that of the corresponding reverse collision. Violation of this condition may produce unphysical equilibrium states, leading to incorrect distributions of translational and internal energies or inaccurate relaxation rates.

On the other hand, in studies focused on constructing a collision kernel, Pullin proposed an alternative kinetic model in which every degree of freedom participates in the energy exchange during each collision¹⁹, and the detailed balance principle is satisfied. This model provides a more physically realistic description of rotation-translation energy exchange. In Pullin’s original model, the energy exchange between rotational and translational modes is represented by five Beta-distributed variates, which can be readily implemented in DSMC simulations. However, this model is computationally expensive. To reduce the computational cost, a simplified variant was introduced employing only three Beta-distributed variates, in which the sum of the rotational energies of the colliding pair is treated as a whole, and the post-collision rotational energy is uniformly distributed²⁰. Another simplified model also employs three Beta-distributed variates, in which only a portion of the translational energy participates in the exchange, and has been applied to vibration-translation energy exchange in DSMC simulations²². Compared with the BL model, these models offer a more physically realistic description of energy exchange; however, their higher computational cost limit their practical use in DSMC simulations. Moreover, the free parameter in the Pullin

model for VHS molecules has not been well established. Consequently, comparative studies on the accuracy and efficiency of the Pullin and BL models remain limited.

Recently, a new rotational-translational distribution function based on Pullin model has been proposed, in which the relationship between the model parameters and the relaxation process is established through the relaxation rates of macroscopic quantities²⁷. In this work, we employ this relation to determine the model parameters for VHS molecules within Pullin's framework and implement the model in the DSMC method. The performance of Pullin's model and its simplified variant is then assessed against that of the BL model through a series of numerical simulations. The remainder of this paper is organized as follows. Section II provides a brief review of Pullin model, its simplified variant, and an energy partition parameter suitable for the VHS model. Section III introduces the collision procedure in the DSMC method and outlines the implementation of the Pullin model within DSMC framework, compared with the BL model. Section IV presents numerical simulations of several typical rarefied gas flows to offer a direct comparison of accuracy and efficiency. Finally, concluding remarks are given in Section V.

II. RESTRICTED ENERGY EXCHANGE SCHEME

A. Review of the Pullin model

The microscopic state of the gas is described by the density distribution function $f(\mathbf{c}, \mathbf{x}, t, \mathbf{e})$, where t , \mathbf{x} , \mathbf{c} , and \mathbf{e} denote the time, position vector, particle velocity, and particle internal energy, respectively. In the absence of external forces, the evolution of f is governed by the reduced generalized Boltzmann equation¹⁹, given by

$$\frac{\partial (nf)}{\partial t} + \mathbf{c} \frac{\partial (nf)}{\partial \mathbf{x}} = Q(f, f), \quad (1)$$

where n is the number density, and the bilinear collision operator $Q(f, f)$ describes binary particle collisions. The operator takes the form as

$$Q(f, f) = n^2 \int \int \cdots \int \left[f'_1 f'_2 J - f_1 f_2 \right] c_r I(\mathbf{e}|\mathbf{e}') d\mathbf{e}' d\Omega' d\mathbf{c}_2 d\mathbf{e}_2, \quad (2)$$

where $\mathbf{e} = (e_1, e_2, e_t)$ represents the components of the internal energy, the factor $J = (e_1 e_2 / e'_1 e'_2)^{\zeta-1}$ with $\zeta = v/2$, and v denoting the internal degrees of freedom. Here, c_r is the relative speed, $d\Omega'$ is the unit solid angle, and $I(\mathbf{e}|\mathbf{e}')$ is the scattering kernel. The

scattering kernel $I(\mathbf{e}|\mathbf{e}')$ satisfies the detailed balancing relation if inverse collisions exist, namely,

$$e_t e_1^{\zeta-1} e_2^{\zeta-1} I(\mathbf{e}|\mathbf{e}') = e'_t e'_1^{\zeta-1} e'_2^{\zeta-1} I(\mathbf{e}'|\mathbf{e}). \quad (3)$$

To simplify the description of momentum and energy exchange during collisions, the scattering kernel I is assumed to separate into independent velocity and energy scattering processes, which is

$$I(\mathbf{e}|\mathbf{e}') = R(\mathbf{e}|\mathbf{e}') \sigma(\chi), \quad (4)$$

where σ is the cross section, χ is the polar deflection angle, and R is the energy scattering kernel. Notice that the decoupling of scattering and internal energy exchange is also consistent with the BL and other phenomenological models. Substituting Eq.(4) into the collision operator (Eq.(2)) yields a model Q , in which the monatomic geometrical scattering properties during collisions are retained and the polyatomic effects (internal-translational energy exchange) are represented phenomenologically through an appropriate choice of R .

For the cross section σ , consider the inverse-power-law molecules with intermolecular potential $V = a/r^\alpha$, where r is the particle separation and a is a constant. For the energy scattering kernel R , substituting the separated form (Eq.(4)) of I into the detailed balance relation (Eq.(3)) leads to the following condition

$$e_t^{\eta-1} e_1^{\zeta-1} e_2^{\zeta-1} R(\mathbf{e}|\mathbf{e}') = e'_t^{\eta-1} e'_1^{\zeta-1} e'_2^{\zeta-1} R(\mathbf{e}'|\mathbf{e}), \quad (5)$$

where $\eta = 2 - 2/\alpha$. In addition, the energy scattering kernel R must satisfy the following requirements: (1) Energy conservation: $e_0 = e_1 + e_2 + e_t = e'_1 + e'_2 + e'_t = e'_0$. (2) Non-negativity: $R \geq 0$. (3) Normalization: for all \mathbf{e} , $\iint R(\mathbf{e}|\mathbf{e}') d\mathbf{e}' = 1$.

It is generally difficult to construct an explicit formulation for R . Pullin¹⁹ introduced an l -dimensional random vector $\mathbf{s} = (s_1, s_2, \dots, s_l)$ with probability density $h(\mathbf{s}) = \prod_{i=1}^l h_i(s_i)$ such that $\iint h(\mathbf{s}) d\mathbf{s} = 1$, where $d\mathbf{s} = ds_1 ds_2 \dots ds_l$. Using this representation, an alternative expression for R can be written as

$$R(\mathbf{e}|\mathbf{e}') d\mathbf{e}' = \iint_v h(\mathbf{s}) d\mathbf{s}, \quad (6)$$

where $h(\mathbf{s})$ is defined by five Beta distribution functions as

$$h(\mathbf{s}) = \left[\prod_{j=1}^2 \beta \langle s_j | \phi\zeta, (1-\phi)\zeta \rangle \right] \beta \langle s_3 | \psi\eta, (1-\psi)\eta \rangle \beta \langle s_4 | \phi\zeta, \phi\zeta \rangle \beta \langle s_5 | 2\phi\zeta, \psi\eta \rangle. \quad (7)$$

Here, $0 < \phi < 1$ and $0 < \psi < 1$ are arbitrary functions (model parameters) of total energy e_0/kT' and viscosity temperature index ω , where T' is any reference temperature. The Beta distribution with parameters μ_1 and μ_2 is defined as

$$\beta \langle z | \mu_1, \mu_2 \rangle = \frac{1}{B(\mu_1, \mu_2)} z^{\mu_1-1} (1-z)^{\mu_2-1}, \quad (8)$$

where $B(\mu_1, \mu_2)$ is the complete Beta function.

With different values of μ_1 and μ_2 , the Beta distribution can be used to collect and redistribute the energies among various degrees of freedom and between molecules. According to the collision operator Eqs.(1) and (7), for inverse-power-law molecules, the post-collision molecular energies in the center-of-mass system can be expressed as

$$\begin{aligned} e'_1 &= (1-s_1)e_1 + s_4s_5e_a, \\ e'_2 &= (1-s_2)e_2 + (1-s_4)s_5e_a, \\ e'_t &= (1-s_3)e_t + (1-s_5)e_a, \\ e_a &= s_1e_1 + s_2e_2 + s_3e_t, \end{aligned} \quad (9)$$

where e_t and e_i denote the pre-collision translational and rotational energies of the molecules, while e'_t and e'_i represent the corresponding post-collision translational and rotational energies. The random variates s_i are sampled from the Beta distributions given as

$$\begin{aligned} \beta \langle s_j | \phi\zeta, (1-\phi)\zeta \rangle, & j = 1, 2, \\ \beta \langle s_3 | \psi\eta, (1-\psi)\eta \rangle, \\ \beta \langle s_4 | \phi\zeta, \phi\zeta \rangle, \\ \beta \langle s_5 | 2\phi\zeta, \psi\eta \rangle, \end{aligned} \quad (10)$$

with ϕ and ψ being model parameters.

Furthermore, the post-collision rotational energies tend to be equally distributed between the two molecules, and it can be assumed that they are effectively partitioned equally²⁰. Under this assumption, the rotational energies of particles e_1 and e_2 are first treated as a whole, and the total e_r is subsequently redistributed equally between them. Consequently, the post-collision energies can be expressed as

$$\begin{aligned} e'_t &= (1-s_1)e_t + (1-s_3)(s_1e_t + s_2e_r), \\ e'_r &= (1-s_2)e_r + s_3(s_1e_t + s_2e_r), \\ e_r &= e_1 + e_2, e'_1 = \mathcal{R}e'_r, e'_2 = (1-\mathcal{R})e'_r, \end{aligned} \quad (11)$$

where \mathcal{R} is a uniformly distributed random number in $(0, 1)$, the random variates s_i are sampled from Beta distributions as

$$\begin{aligned} & \beta \langle s_1 | \psi \eta, (1 - \psi) \eta \rangle, \\ & \beta \langle s_2 | 2\phi, 2(1 - \phi) \rangle, \\ & \beta \langle s_3 | 2\phi, \psi \eta \rangle. \end{aligned} \quad (12)$$

For this simplified variant of the Pullin model, the detailed balance principle is also satisfied²⁰.

Once the values of ϕ and ψ are specified, both models above are fully determined, and the relation between these parameters and the relaxation process is discussed in the following subsection.

B. Selection of model parameters

In the Pullin model, two model parameters, ϕ and ψ , must be specified within the calculation framework. Based on the Chapman-Enskog expansion of the macroscopic transport coefficients, a specific formulation of these parameters for hard-sphere (HS) molecules was proposed¹⁹, i.e.,

$$\begin{cases} \psi = \phi = \phi_0, \omega < 1, \\ \psi = \phi = 0, \omega > 1. \end{cases} \quad (13)$$

When $\omega < 1$, the relationship between the model parameter ϕ_0 and rotational collision number Z is given as

$$\phi_0 = \frac{8(2 + \nu)}{5\pi} \frac{1}{Z}. \quad (14)$$

For the VHS molecules, Pullin did not establish a direct relationship between the parameters ϕ and ψ and the relaxation properties, which may limit the broader applicability of this model. Recently, an explicit formulation of these parameters is derived based on the equipartition theorem, in which the translational and rotational energies of two colliding particles are redistributed in proportion to their respective degrees of freedom²⁷. Under this framework, the relaxation of translational and rotational temperatures is governed by

$$\frac{\partial T_{tr}}{\partial t} = \frac{5 \cdot 4^\eta \sqrt{\pi} n \left(\frac{m}{k T_{tr}} \right)^{\frac{3}{2} - \eta} (T - T_{tr}) c_{r,ref}^{4-2\eta} \cdot \sigma_{ref} \Gamma(1 + \eta) \phi \psi}{3(2\phi + \eta\psi)}, \quad (15)$$

$$\frac{\partial T_{rot}}{\partial t} = \frac{5 \cdot 4^\eta \sqrt{\pi} n \left(\frac{m}{kT_{tr}} \right)^{\frac{3}{2}-\eta} (T - T_{rot}) c_{r,ref}^{4-2\eta} \cdot \sigma_{ref} \Gamma(1+\eta) \phi \psi}{3(2\phi + \eta\psi)}, \quad (16)$$

where m is the molecular mass, σ_{ref} is the collision cross section, and Γ is the gamma function. Meanwhile, the relaxation of the stress tensor is given by

$$\frac{\partial p_{\langle ij \rangle}}{\partial t} = -\frac{2^{1+2\eta} \sqrt{\pi} n \left(\frac{m}{kT_{tr}} \right)^{\frac{3}{2}-\eta} c_{r,ref}^{4-2\eta} \sigma_{ref} \Gamma(1+\eta) (1+\eta)}{15} p_{\langle ij \rangle}. \quad (17)$$

According to the definition of relaxation rate for macroscopic variables, the Eqs.(16) and (17) can be rewritten in the standard form, i.e.,

$$\begin{aligned} \frac{\partial T_{rot}}{\partial t} &= \frac{T - T_{rot}}{\tau_{rot}}, \\ \frac{\partial p_{\langle ij \rangle}}{\partial t} &= -\frac{p_{\langle ij \rangle}}{\tau_{tr}}, \end{aligned} \quad (18)$$

where τ_{rot} and τ_{tr} denote the rotational and translational relaxation times, respectively. The rotational collision number Z is defined as $Z = \tau_{rot}/\tau_{tr}$. Therefore, based on the relaxation rate of temperature and stress tensor, the rotational collision number Z (relax to the total temperature T) can be expressed as

$$Z = \frac{2(1+\eta)(2\phi + \eta\psi)}{25\phi\psi}. \quad (19)$$

In Pullin's partition function Eq.(7), the terms $\phi\zeta$ and $\psi\eta$ denote the fractions of internal and translational energies, respectively. According to the equipartition theorem, the energy associated with each mode is distributed in proportion to its degrees of freedom. Accordingly, for a diatomic gas, the relation between ψ and ϕ can be determined as follows

$$\psi = \frac{3}{2\eta}\phi. \quad (20)$$

Consequently, the model parameters ψ and ϕ can be directly determined from the rotational collision number Z as

$$\begin{aligned} \phi &= \frac{14\eta(1+\eta)}{75Z}, \\ \psi &= \frac{7(1+\eta)}{25Z}. \end{aligned} \quad (21)$$

It should be noted that the values of ϕ and ψ must remain within the range $(0, 1)$, which imposes a lower bound on the rotational collision number Z . For nitrogen, this constraint requires that Z must be greater than 0.906752. From a physical perspective, the rotational collision number is typically greater than unity, indicating that the present formulation is physically reasonable. Although these parameters are derived from the Pullin model, they are likewise employed in the simplified variant of the Pullin model used in this study.

III. IMPLEMENTATION OF THE ENERGY EXCHANGE MODEL IN THE DSMC METHOD

A. The direct simulation Monte Carlo method

The DSMC method is a stochastic, particle-based numerical approach for solving the Boltzmann equation²⁸, in which the velocity distribution function is approximated by a large number of simulated particles. Using an operator splitting scheme, the generalized Boltzmann equation Eq.(1) is decomposed into free-transport and collision steps, i.e.,

$$\begin{cases} \frac{\partial (nf)}{\partial t} + \mathbf{c} \frac{\partial (nf)}{\partial \mathbf{x}} = 0, \\ \frac{\partial (nf)}{\partial t} = Q(f, f). \end{cases} \quad (22)$$

In the DSMC method, the free-transport step corresponds to free molecular motion, while the collision step simulates intermolecular interactions through stochastic sampling. During the free-transport step, the motion of each particle is computed using a Lagrangian tracking approach, in which each particle is advanced according to its instantaneous velocity \mathbf{c}_i over a discrete time interval Δt , i.e.,

$$\begin{aligned} \mathbf{r}_i^{n+1} &= \mathbf{r}_i^n + \mathbf{c}_i \Delta t, \\ d(m_i \mathbf{c}_i) / dt &= \mathbf{C}(\mathbf{c}_i, e_i), \end{aligned} \quad (23)$$

where subscript “ i ” denotes the particle index, \mathbf{r}_i and \mathbf{c}_i represent the position and velocity of the particle i , respectively, m is the mass of the particle, and \mathbf{C} represents the binary collision process each particle undergoes during the time step. As a core component of the DSMC method, the collision algorithm determines the post-collision velocities and energies of selected particle pairs based on their pre-collision states. Among various approaches, the No Time Counter (NTC) scheme^{8,29} is the most widely adopted. In this scheme, the number of candidate collision pairs, N_c , within each time step Δt is estimated using the maximum collision probability. The value of N_c is given by

$$N_c = \frac{1}{2} N (N - 1) F_N (\sigma_T c_r)_{\max} \Delta t / V_c \quad (24)$$

where N is the number of simulated particles in the computational cell, F_N denotes the ratio of real molecules to simulated particles, σ_T represents the total collision cross section, c_r is the relative velocity between two colliding particles, and V_c is the volume of the computational

cell. Since the number of collisions must be an integer, the actual number of collision pairs tested, $N_{c,\text{test}}$, is taken as $\lfloor N_c \rfloor$ with an additional collision included with probability $N_c - \lfloor N_c \rfloor$. Each of the $N_{c,\text{test}}$ pairs of particles is selected at random regardless of position in the cell, and then the candidate pairs are chosen to collide with a probability

$$p_c = \frac{\sigma_{TCr}}{(\sigma_{TCr})_{\max}}, \quad (25)$$

where σ_{TCr} represents the product of the total collision cross-section and the relative velocity of the selected particle pair. The quantity $(\sigma_{TCr})_{\max}$ is initially assigned a suitable reference value within the computational cell and is subsequently updated if σ_{TCr} for any selected particle pair exceeds this threshold. By comparing the collision probability p_c with a uniformly distributed random number $\mathcal{R} \in (0, 1)$, an acceptance-rejection (AR) procedure is used to determine whether the candidate particle pair actually collides. If accepted, this particle pair undergoes either an elastic collision (the change of particle speed) or an inelastic collision (the exchange of translational energy and internal energy), in which translational energy is exchanged with internal energy and redistributed between the different degrees of freedom.

B. Implementation of the Borgnakke-Larsen model

In the DSMC method, the BL model^{8,18} is commonly employed to describe energy exchange between translational and internal modes during collisions. Within the BL framework, the total energy e_c of a collision pair, consisting of both translational and internal components, is strictly conserved. After the collision, the internal energy is redistributed according to an equilibrium distribution based on the combined translational and internal energies. The relaxation rate is governed by the ratio of inelastic to elastic collisions, ensuring consistency with the prescribed macroscopic relaxation behavior. In practice, the inelastic collision probability p_i is typically defined as $p_i = 1/Z_{\text{BL}}$, where Z_{BL} denotes the model-specific relaxation number. It should be emphasized, however, that the definition of Z_{BL} may differ from the collision number Z employed in other models, such as Pullin's model. In the present work, the analysis is restricted to rotational energy, and the serial BL procedure²³ is adopted. Specifically, each particle in a collision pair is independently tested for inelastic participation. When particle A is selected, the collision type is determined based

on the inelastic collision probability p_i . If an inelastic collision occurs, the collision energy is defined as $e_c = e_t + e_1$. The post-collision rotational energy e_i lies within the interval $[0, e_c]$ and is generated by sampling from a uniform random variate \mathcal{R}_1 . The probability of a given rotational energy, normalized by its maximum value, is expressed as

$$\frac{p}{p_{\max}} = \left(\frac{\zeta_{\text{rot}}/2 + 1/2 - \omega}{\zeta_{\text{rot}}/2 - 1} \frac{e_i}{e_c} \right)^{\zeta_{\text{rot}}/2-1} \left[\frac{\zeta_{\text{rot}}/2 + 1/2 - \omega}{3/2 - \omega} \left(1 - \frac{e_i}{e_c} \right) \right]^{3/2-\omega}, \quad (26)$$

where ζ_{rot} is the rotational degrees of freedom. The post-collision rotational energy is then given by $e_i = \mathcal{R}_1 e_c$. Another random number \mathcal{R}_2 is generated for comparison. If $\mathcal{R}_2 \leq p/p_{\max}$, the rotational energy e_i is accepted as the post-collision rotational energy e_1' of particle A; otherwise, a new value of e_i is sampled until acceptance. The post-collision translational energy of particle A is then determined by $e_t' = e_c - e_1'$. Subsequently, particle B is subjected to the same probabilistic criterion p_i to decide whether its collision is elastic or inelastic. The redistributed translational energy from the first step is combined with the rotational energy of particle B to define a new collision energy $e_c' = e_t' + e_2$. The post-collision rotational energy of particle B is sampled from a uniform random variate \mathcal{R}_3 , until acceptance. The final post-collision rotational energy of particle B is then given by $e_2' = \mathcal{R}_3 e_c'$, and the post-collision translational energy is given by $e_t'' = e_c' - e_2'$. Therefore, the magnitude of the post-collision relative velocity c_r' between the molecules can be expressed as $c_r' = \sqrt{2e_t''/m_r}$, where m_r is the reduced mass of the collision pair. The post-collision velocities of particle pair are updated as follows

$$\begin{aligned} \mathbf{c}_1' &= \frac{1}{2}[(\mathbf{c}_1 + \mathbf{c}_2) - c_r' \omega], \\ \mathbf{c}_2' &= \frac{1}{2}[(\mathbf{c}_1 + \mathbf{c}_2) + c_r' \omega], \end{aligned} \quad (27)$$

where \mathbf{c}_1 and \mathbf{c}_2 denote the pre-collision velocities of the two colliding particles A and B, \mathbf{c}_1' and \mathbf{c}_2' represent their post-collision velocities, and ω is a unit vector that defines the direction of the post-collision relative velocity. The vector ω performs a random walk on the unit sphere, which depends on the selected collision model. For the VHS model, ω is given as

$$\omega = (\cos \chi, \sin \chi \cos \theta, \sin \chi \sin \theta)^T, \quad (28)$$

where, in polar coordinates, the cosine of deflection angle χ and azimuth angle θ are uniformly distributed over the intervals $[-1, 1]$ and $[0, 2\pi]$, respectively. That is,

$$\cos \chi = 2\mathcal{R}_4 - 1, \quad \theta = 2\pi\mathcal{R}_5. \quad (29)$$

Although the BL model has been widely applied and shows good agreement in practical simulations, it is physically inconsistent because only a subset of collisions is treated as inelastic. To enhance the physical fidelity of the model, Bird proposed a modified variant of the BL model⁸, in which all collisions are regarded as inelastic, but only a prescribed fraction p_i of the calculated change in rotational energy is transferred during each collision. In practical implementation, this means that all colliding particles are treated as undergoing inelastic collisions, thereby eliminating the need for probabilistic selection. Specifically, the post-collision rotational energy of particle A is calculated as $e_1'' = e_1(1 - p_i) + e_1'p_i$, and the corresponding post-collision translational energy for the collision pair is then given by $e_t' = e_c - e_1''$. Subsequently, the post-collision rotational energy of particle B is computed as $e_2'' = e_2(1 - p_i) + e_2'p_i$, and the final post-collision translational energy for the collision pair is given by $e_t'' = e_c' - e_2''$. While this modification preserves the relaxation rate, it does not satisfy the principle of detailed balance¹⁹.

C. Implementation of the Pullin model

The Pullin model is straightforward to implement within the DSMC framework, requiring modifications only to the colliding particles. It allows for the computation of the translational and rotational energies of each particle after collision, while the remaining parts of the Pullin model remain consistent with the conventional DSMC method. The computational procedures for the Pullin and BL models within the DSMC framework are illustrated in the Fig.1. It should be noted that the definition of rotational collision number in the Pullin model Z differs from that in the BL model Z_{BL} ; to ensure consistent results, this difference must be analyzed first. Moreover, both the Pullin model and its simplified variant rely solely on sampling from Beta distributions (five or three), with only the input parameters differing. Therefore, the following section provides a detailed discussion of the rotational collision number in the Pullin model and the associated Beta distribution sampling procedure.

In the Pullin model, the rotational collision number is defined directly in a form consistent with experimental measurements^{30,31}, i.e.,

$$Z = \frac{\tau_{rot}}{\tau_{tr}}, \quad (30)$$

where τ_{tr} denotes the translational relaxation time, defined as μ/p , with μ being the viscosity coefficient and p the pressure. In the BL model, the definition of the rotational collision

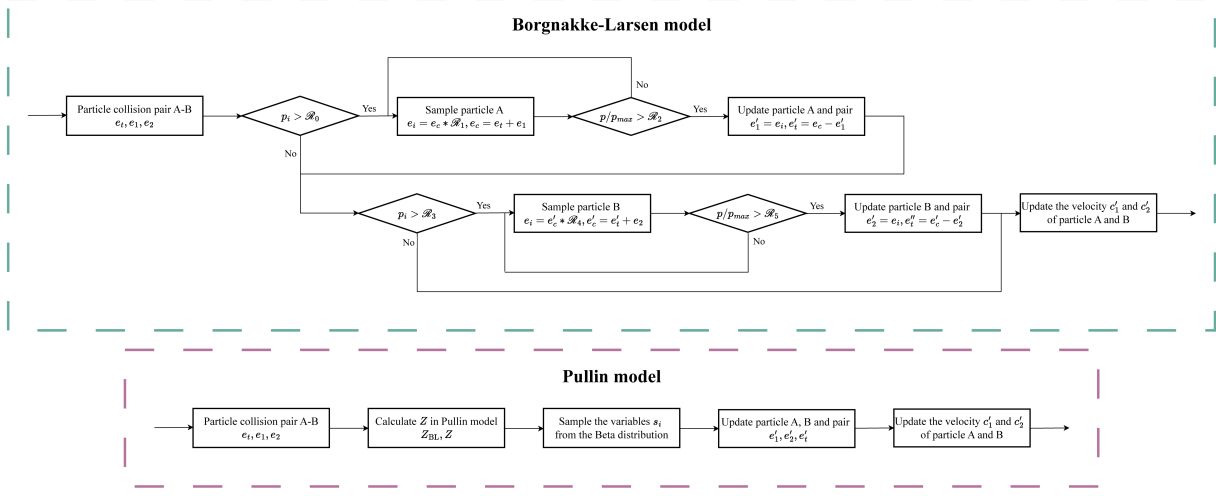


FIG. 1. Comparison of the implementation procedures of the BL and Pullin models within the DSMC framework. Top: BL model; bottom: Pullin model.

number Z_{BL} is consistent with that of the Pullin model; however, the definition of the translational relaxation time τ_{tr} differs and depends on the employed collision model. For the widely used VHS model, the translational relaxation time is given by

$$\tau_{tr,VHS} = \frac{(5 - 2\omega)(7 - 2\omega)}{30} \frac{\mu}{p}. \quad (31)$$

To enable a consistent comparison between the Pullin and BL models, the collision number Z is expressed in terms of the collision number Z_{BL} through the relationship

$$Z = \frac{\tau_{rot}}{\tau_{tr}} = \frac{\tau_{rot}}{\tau_{tr,VHS}} \cdot \frac{\tau_{tr,VHS}}{\tau_{tr}} = \frac{(5 - 2\omega)(7 - 2\omega)}{30} Z_{BL}. \quad (32)$$

If the Pullin model is employed in the DSMC method, the rotational collision number Z_{BL} must be converted to the corresponding rotational collision number Z in the Pullin model.

Several algorithms have been proposed for the computer generation of random variates following the $\beta(z | \mu_1, \mu_2)$ distribution. Among the most widely used are Jöhnk's method³² and Cheng's algorithm³³, both of which are applicable for all shape parameters $\mu_1 > 0, \mu_2 > 0$ and capable of generating Beta-distributed variates over a wide range of parameter values. Jöhnk's method, in particular, is simple and effective, relying on the transformation of uniform random numbers. The procedure can be summarized as follows: two independent Uniform(0, 1) random numbers \mathcal{R}_{01} and \mathcal{R}_{02} are first generated, and then transformed via $V_1 = \mathcal{R}_{01}^{1/\mu_1}$ and $V_2 = \mathcal{R}_{02}^{1/\mu_2}$. The sum $W = V_1 + V_2$ is then computed; If $W \leq 1$, the Beta-distributed random variate is obtained as $z = V_1/W$; otherwise, the process is repeated. This

algorithm ensures that the resulting random variate z follows the $\beta(z | \mu_1, \mu_2)$ distribution. Its generality and ease of implementation make it well suited for use in the Pullin model within the DSMC framework.

IV. NUMERICAL SIMULATIONS

To evaluate the predictive capability of the Pullin model across a wide range of nonequilibrium phenomena, five typical test cases are simulated and analysed: zero-dimensional (0-D) rotational relaxation of nitrogen, one-dimensional (1-D) planar Couette flow and normal shock structure, two-dimensional (2-D) hypersonic flow around a circular cylinder, and three-dimensional (3-D) hypersonic flow around an X38-like vehicle. The Pullin model is implemented within the DSMC framework, and the results are compared with those obtained using the BL model. Unless otherwise specified, all Pullin and BL results discussed in the following are obtained from the DSMC codes DSMC0R and DS1 developed by Bird⁸, or from the open-source solver SPARTA³⁴.

For nitrogen flow, the variable hard sphere (VHS) model is adopted, in which the viscosity μ depends on the translational temperature T_{tr} according to the power-law relation

$$\mu = \mu_{ref} \left(\frac{T_{tr}}{T_{ref}} \right)^\omega. \quad (33)$$

In all subsequent simulations, the reference viscosity is $\mu_{ref} = 1.656 \times 10^{-5} \text{ Pa}\cdot\text{s}$ with a power-law exponent $\omega = 0.74$, and the corresponding reference diameter $d_{ref} = 4.17 \times 10^{-10} \text{ m}$ at $T_{ref} = 273 \text{ K}$. Unless otherwise stated, the freestream Knudsen number Kn is defined as $\text{Kn} = \lambda/L_{ref}$, where the mean free path λ for the VHS model is expressed as

$$\lambda = \frac{1}{\sqrt{2\pi} d_{ref}^2 n \left(\frac{T_{ref}}{T_{tr}} \right)^{\omega-0.5}}. \quad (34)$$

A. Rotational relaxation of nitrogen

The rotational relaxation of nitrogen is a typical 0-D nonequilibrium flow problem, widely employed to examine the energy exchange between translational and rotational modes^{8,21}. The system is initialized in a strongly nonequilibrium state: 100,000 simulated particles are confined within a single isolated computational cell, with a translational temperature

of $T_{tr} = 500\text{K}$ and a rotational temperature of $T_{rot} = 0\text{K}$, corresponding to zero rotational energy. As relaxation proceeds, the system asymptotically approaches thermal equilibrium at $T_{eq} = 300\text{K}$. In the present simulation, the rotational collision number in the BL model is maintained at a constant value of $Z_{BL} = 5$, while the corresponding parameter Z in the Pullin model is evaluated from Eq. (32).

In this simulation, the time evolution of the rotational and translational temperatures can be derived analytically⁸. The predicted value of the rotational temperature is given by

$$T_{rot} = 300[1 - \exp(-vt/5)], \quad (35)$$

while the translational temperature is obtained analogously as

$$T_{tr} = 300 + 200 \exp(-vt/5), \quad (36)$$

where v denotes the collision frequency. During relaxation, the translational temperature T_{tr} decreases monotonically, whereas the rotational temperature T_{rot} increases monotonically, with both asymptotically approaching 300K. At equilibrium, the molecular speed distribution $f_{\beta c}$ takes the Maxwell form

$$f_{\beta c} = \frac{4}{\sqrt{\pi}} \beta^2 c^2 \exp(-\beta^2 c^2), \quad (37)$$

while the rotational energy distribution $f_{e_{rot}/(kT)}$ of nitrogen is given by

$$f_{e_{rot}/(kT)} = \exp(-e_{rot}/kT). \quad (38)$$

Figure 2 illustrates the temporal evolution of the rotational temperature during the relaxation process. The results from the Pullin model and its simplified variant agree well with the analytical solution. For comparison, results from the BL model and its modified variant are also included; both exhibit reasonable agreement with the Pullin model and the analytical solution. At equilibrium, the velocity distribution functions from the four different models are shown in Fig. 3(a) and compared with the Maxwell distribution $f_{\beta c}$ at the equilibrium temperature T_{eq} , with all four models demonstrating satisfactory agreement. Figure 3(b) presents the rotational energy distribution functions on a logarithmic scale. The Pullin model, its simplified variant, and the BL model exhibit an exponential dependence on the rotational energy and agree closely with the theoretical solution $f_{e_{rot}/(kT)}$, whereas the modified BL model fails to reproduce the theoretical distribution at equilibrium, primarily

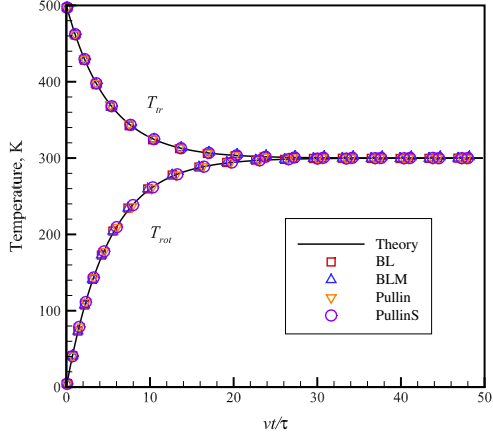


FIG. 2. Rotational relaxation in nitrogen gas. Squares: BL model; triangles: modified BL model; gradients: Pullin model; circles: simplified Pullin model; solid line: analytical solution.

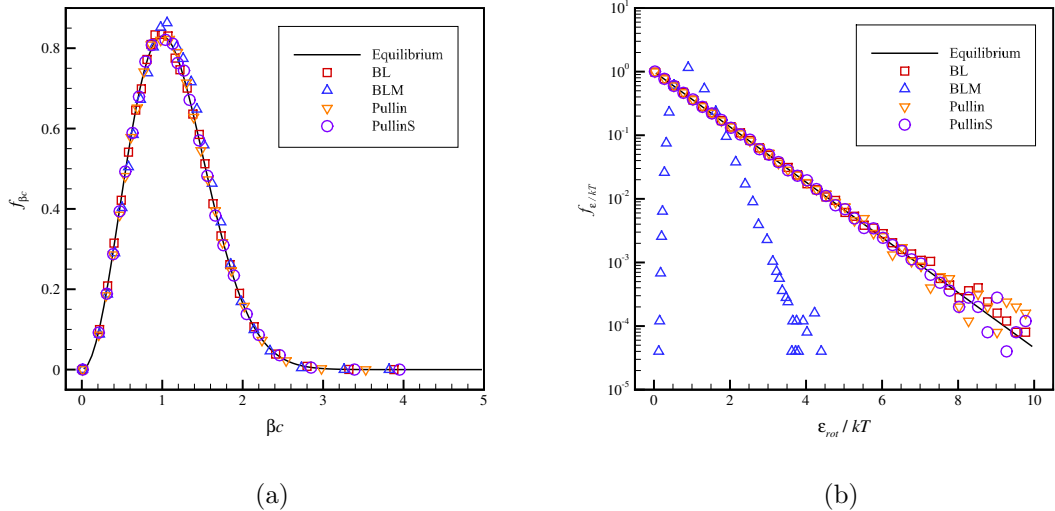


FIG. 3. Equilibrium distributions of nitrogen molecules: (a) molecular speeds and (b) rotational energies. Squares: BL model; triangles: modified BL model; gradients: Pullin model; circles: simplified Pullin model; solid line: theoretical solution.

because it does not satisfy the principle of detailed balance. These results demonstrate that the Pullin model, its simplified variant, and the BL model accurately capture the nonequilibrium energy exchange between translational and rotational modes.

The computational times for all test cases obtained using different methods are summarized in Table I. All computations are performed using a single core of an AMD Ryzen

TABLE I. Comparison of computational times for different rotational energy relaxation models.

Exchange model	BL	BLM	Pullin	PullinS
Total CPU time (s)	424.549	470.266	594.484	548.813

9 5900X processor. The results show that the Pullin model requires approximately 40% more computational time than the BL model, primarily due to the additional sampling of Beta distributions. The simplified Pullin model, which involves fewer Beta distribution samplings, reduces the computational time by about 7.7% compared to the full Pullin model while maintaining comparable accuracy. Overall, both the Pullin model and its simplified variant are computationally more demanding than the BL model but offer improved physical fidelity in simulating energy exchange processes.

B. Planar Couette flow

The planar Couette flow³⁵ is considered to assess the performance of the Pullin model in shear-driven transport. The configuration consists of a lower plate at $x = 0$ and a parallel upper plate separated by a distance of 10 mean free paths ($h = 10\lambda$). The plates move in opposite directions, each with a velocity of $U_p = 336.89\text{m/s}$. The Knudsen number is set to $\text{Kn} = 0.1$, with the reference length defined as the plate separation h . The working gas is nitrogen, modeled using the VHS model. The initial state is uniform, with a number density of $n_0 = 2.69 \times 10^{25}\text{m}^{-3}$ and translational and rotational temperatures of $T_0 = 273\text{K}$. Both plates are maintained at $T_{wall} = 273\text{K}$ and modeled as fully diffusive walls. The rotational collision number in the BL model is set to $Z_{\text{BL}} = 5$, while the corresponding value Z in the Pullin model is calculated from Eq. (32). The computational domain is divided into 300 uniform cells along the vertical direction, with each computational cell initially containing approximately 2,000 simulated particles. The results are averaged over 10,000 time steps after the system reaches steady state.

Figures 4(a) and 4(b) show the density and velocity profiles, respectively, while Fig. 4(c) presents the translational temperature profile. The heat flux profile is given in Fig. 4(d). Across all flow variables, the results from the Pullin model and its simplified variant agree well with those from the BL model. In particular, the Pullin model reproduces the heat flux profile with high accuracy, a quantity especially sensitive to nonequilibrium effects. These

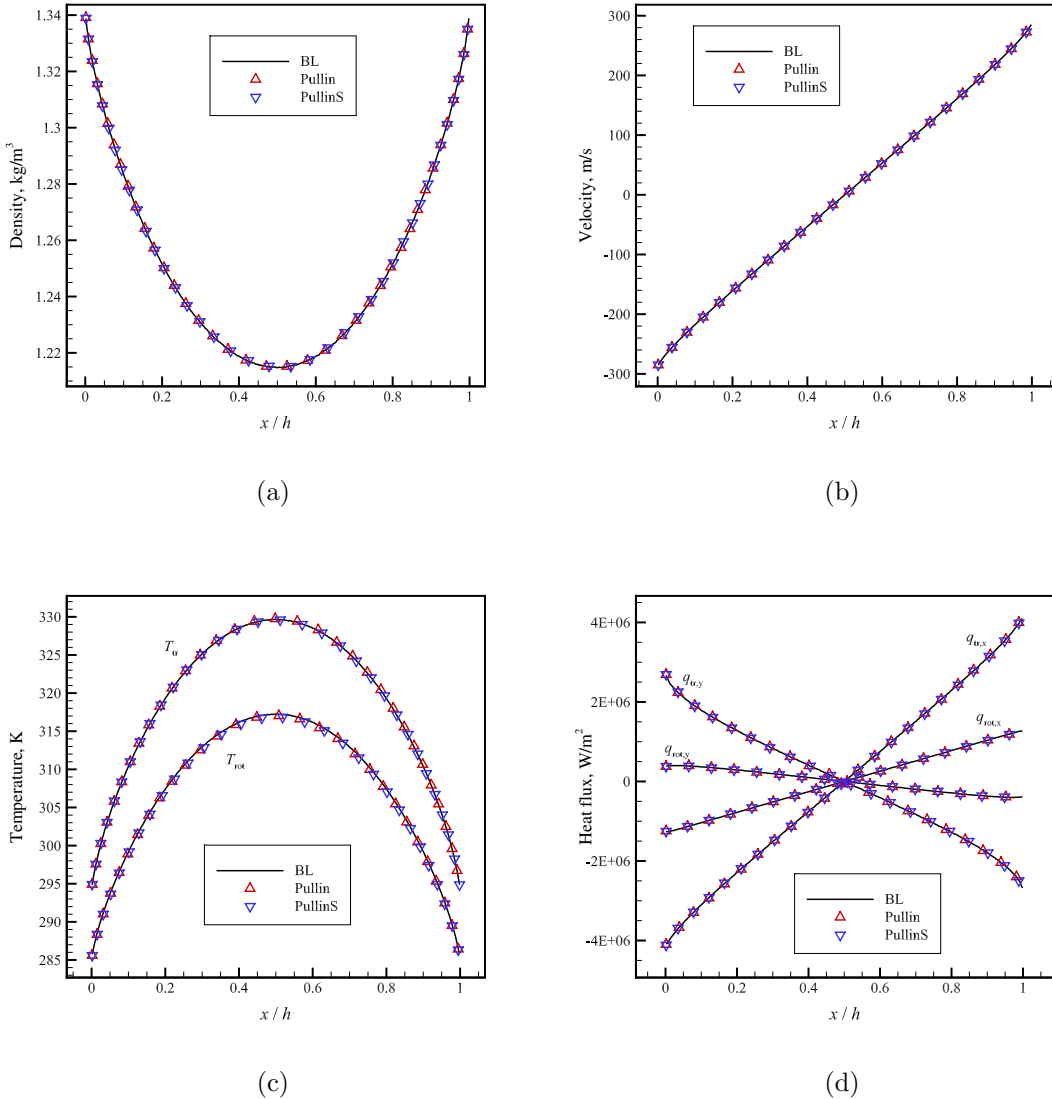


FIG. 4. Couette flow profiles at $\text{Kn} = 0.1$: (a) density; (b) velocity; (c) temperature; (d) heat flux. Triangles: Pullin model; gradients: simplified Pullin model; solid line: BL model.

results demonstrate that the Pullin model provides a reliable description of shear-driven transport phenomena in rarefied gas flows.

C. Normal shock wave

The normal shock wave serves as a fundamental test case for validating the Pullin model under strongly nonequilibrium conditions, as sharp gradients of velocity, density, and temperature develop over only a few mean free paths. Robben and Talbot³⁶ reported experimental

TABLE II. The upstream and downstream parameters of the normal shock wave.

Ma	$n_1(m^{-3})$	$u_1(m/s)$	$T_1(K)$	$n_2(m^{-3})$	$u_2(m/s)$	$T_2(K)$	Z_{BL}	ω
1.53	1.0E20	540.37	300	1.92E20	282.43	402.09	4.0	0.72
2.0	1.0E20	706.37	300	2.67E20	264.89	506.25	4.0	0.72
6.1	1.0E20	2154.43	300	5.29E20	407.32	2452.8	4.4	0.72
10.0	1.0E20	3531.86	300	5.72E20	618.08	6116.25	5.0	0.72

data for nitrogen shock waves, including measurements of both rotational temperature and density. Additional density-profile measurements were obtained by Alsmeyer³⁷, and these datasets have since been widely used for numerical validation, as demonstrated by Boyd³⁸.

Following Alsmeyer's experimental setup, the present study simulates the normal shock wave in nitrogen at upstream Mach numbers of $Ma = 1.53, 2.0, 6.1$, and 10.0 . The upstream conditions are specified as follows: number density $n_1 = 1.0 \times 10^{20} m^{-3}$, translational and rotational temperatures $T_{tr,1} = T_{rot,1} = 300K$, and velocity u_1 determined from the Mach number. The corresponding downstream conditions are obtained from the Rankine-Hugoniot relations and summarized in Table II, which also lists the rotational collision numbers Z_{BL} and viscosity indices ω employed in the simulations. The corresponding value Z in the Pullin model is calculated from Eq. (32). The computational domain extends from $x = -50\lambda_1$ to $x = 50\lambda_1$, where λ_1 is the upstream mean free path, and is discretized into 2,000 uniform cells, with each cell initially containing approximately 2,500 simulated particles. The upstream boundary is treated as an inflow condition, while the downstream boundary is modeled as a specularly reflecting wall moving at the downstream velocity u_2 .

Figure 5 presents the translational and rotational temperature profiles across the shock wave for different Mach numbers. The x coordinate is normalized by the upstream mean free path λ_1 , defined according to the hard-sphere (HS) model as

$$\lambda_1 = \frac{16\mu_1}{5\rho_1 (2\pi RT_1)^{1/2}}, \quad (39)$$

where R is the gas constant, μ_1 and ρ_1 are the upstream viscosity and density, respectively. The upstream viscosity μ_1 is calculated using the reference viscosity $\mu_{ref} = 1.656 \times 10^{-5} \text{ Pa} \cdot \text{s}$ and reference temperature $T_{ref} = 273 \text{ K}$. The translational temperature predicted by the Pullin model differs slightly from that of its simplified variant; however, both are generally in good agreement with the results of the BL model. As the upstream Mach number increases,

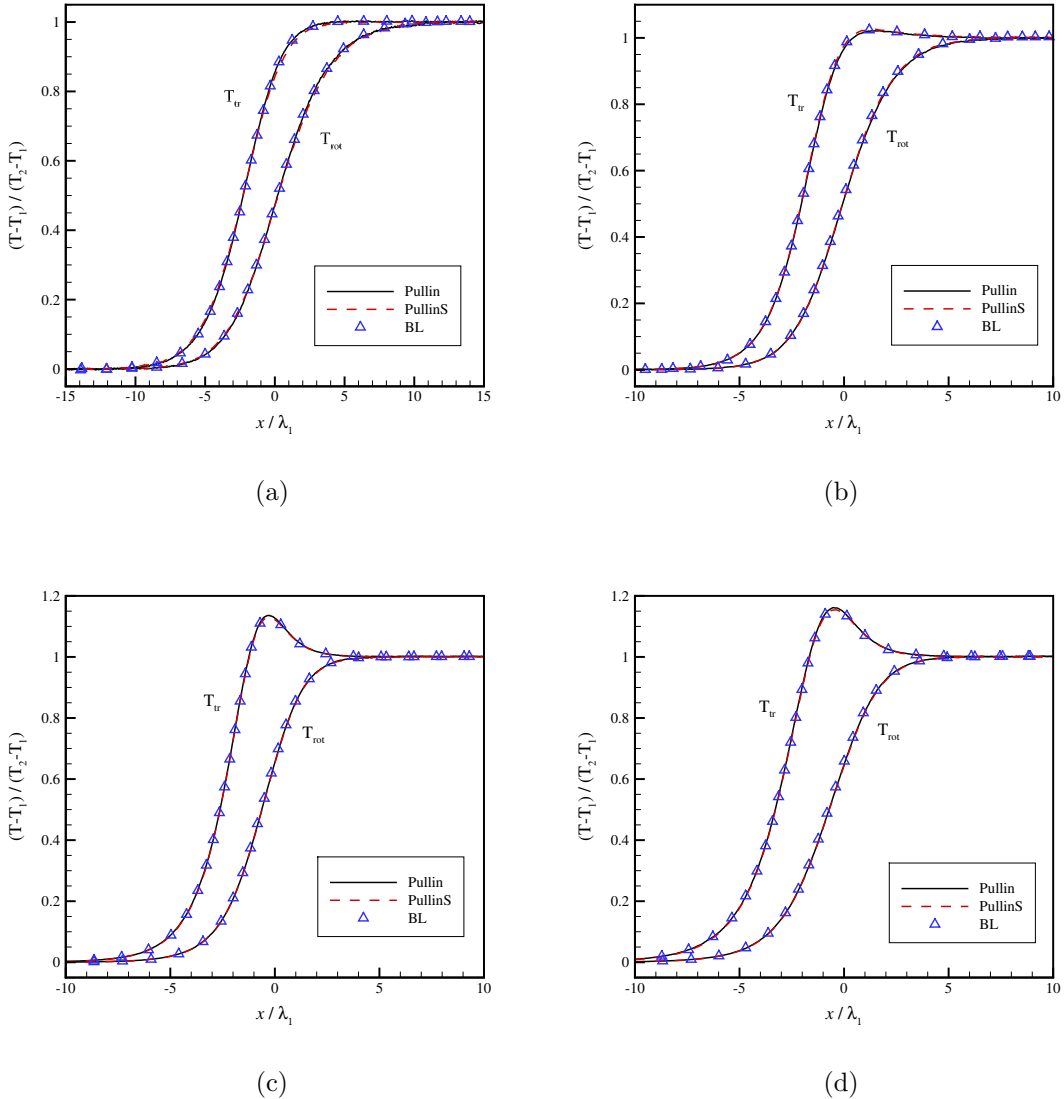


FIG. 5. Temperature profiles of shock waves at different Mach numbers: (a) $\text{Ma} = 1.53$; (b) $\text{Ma} = 2.0$; (c) $\text{Ma} = 6.1$; (d) $\text{Ma} = 10.0$. Solid line: Pullin model; dashed line: simplified Pullin model; triangles: BL model.

the shock wave becomes thicker and nonequilibrium effects become more pronounced. Figure 6 shows the corresponding density profiles across the shock wave. The results from the Pullin model and its simplified variant agree well with those from the BL model as well as with experimental data from Alsmeyer³⁷. Overall, these results demonstrate that the Pullin model and its simplified variant accurately capture the complex nonequilibrium phenomena in normal shock waves.

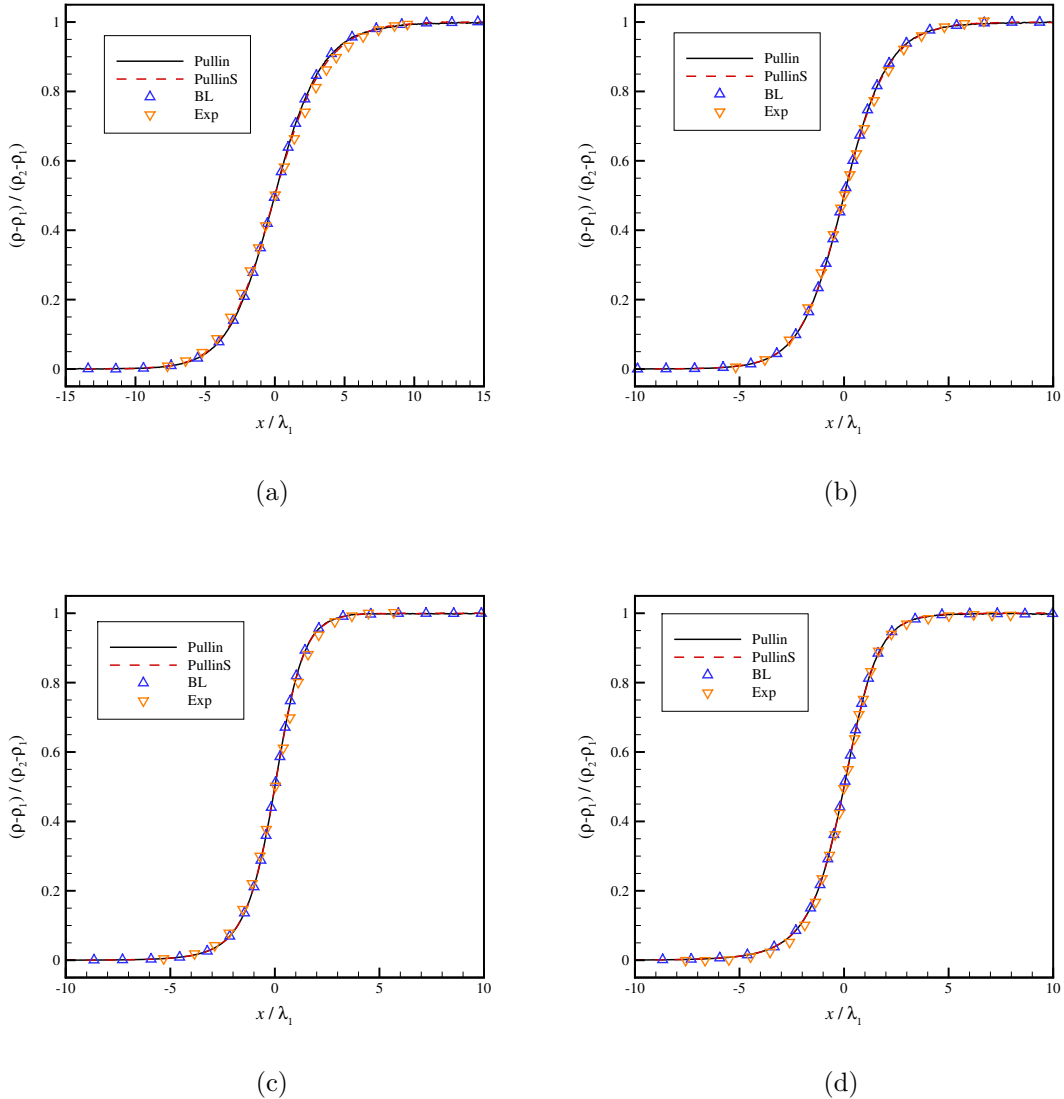


FIG. 6. Density profiles of shock waves at different Mach numbers: (a) $\text{Ma} = 1.53$; (b) $\text{Ma} = 2.0$; (c) $\text{Ma} = 6.1$; (d) $\text{Ma} = 10.0$. Solid line: Pullin model; dashed line: simplified Pullin model; triangles: BL model; gradients: experimental data from Alsmeyer³⁷.

D. Hypersonic flow past a cylinder

The hypersonic flow past a cylinder is a classical benchmark for assessing energy-exchange models in rarefied gas dynamics, characterized by a high-density region ahead of the cylinder and a rarefied wake downstream. In this study, hypersonic flow past a cylinder is simulated at a freestream Mach number of $\text{Ma} = 5$ for four Knudsen numbers: $\text{Kn} = 0.01, 0.1, 1.0$, and 10.0 . The cylinder radius, chosen as the characteristic length, is set to $L_{ref} =$

$R = 1m$. The working gas is nitrogen, with freestream number densities of $1.29438 \times 10^{20} m^{-3}$, $1.29438 \times 10^{19} m^{-3}$, $1.29438 \times 10^{18} m^{-3}$, and $1.29438 \times 10^{17} m^{-3}$ corresponding to the four Knudsen numbers. Both translational and rotational temperatures are initialized at $T_{tr} = T_{rot} = 273K$, and the freestream velocity is $V = 1684.59 m/s$. A fully diffusive wall boundary condition is applied, maintaining a constant wall temperature of $T_{wall} = 500K$. The rotational collision number in the BL model is set to $Z_{BL} = 5$, while the corresponding value Z in the Pullin model is obtained from Eq. (32). Each computational cell is initialized with about 20 simulated particles, and the results are averaged over 40,000 time steps after the flow reaches steady state.

Figures 7-10 compare the translational and rotational temperature contours predicted by the three internal energy relaxation models at four freestream Knudsen numbers. Across all four Knudsen numbers, the translational temperature results from the three models agree well. Similarly, for $Kn = 0.01$ and 0.1 , the rotational temperature predictions are also consistent. However, differences emerge as the Knudsen number increases: at $Kn = 1$ and 10 , the Pullin and BL models exhibit slight discrepancies in the rotational temperature in the wake region behind the cylinder, whereas the Pullin model and its simplified variant remain nearly identical. These flowfield results further indicate that at $Kn = 0.01$, the translational and rotational temperatures are almost equal, suggesting negligible thermal nonequilibrium. As the Knudsen number increases, the difference between translational and rotational temperatures grows, reflecting stronger nonequilibrium effects. Notably, the rotational temperature in the wake progressively rises with Kn , and at $Kn = 10$, it becomes comparable to—or even slightly higher than—that at the stagnation point, demonstrating that nonequilibrium effects are significant in highly rarefied hypersonic flows.

Figure 11 presents a comparison of the surface pressure at different Knudsen numbers, while Figure 12 shows the corresponding surface shear stress. It can be observed that the Pullin model and its simplified variant are in good agreement with the BL model reference solutions. Figure 13 compares the surface heat fluxes for different Knudsen numbers, including the translational and rotational components. Across all four Knudsen numbers, the results from the three models are in good agreement. As the freestream Knudsen number increases, the flow becomes increasingly nonequilibrium, resulting in a gradual decrease in the rotational heat flux and a corresponding increase in the contribution of translational heat flux to the total heat flux. At $Kn = 10$, the rotational heat flux even becomes negative,

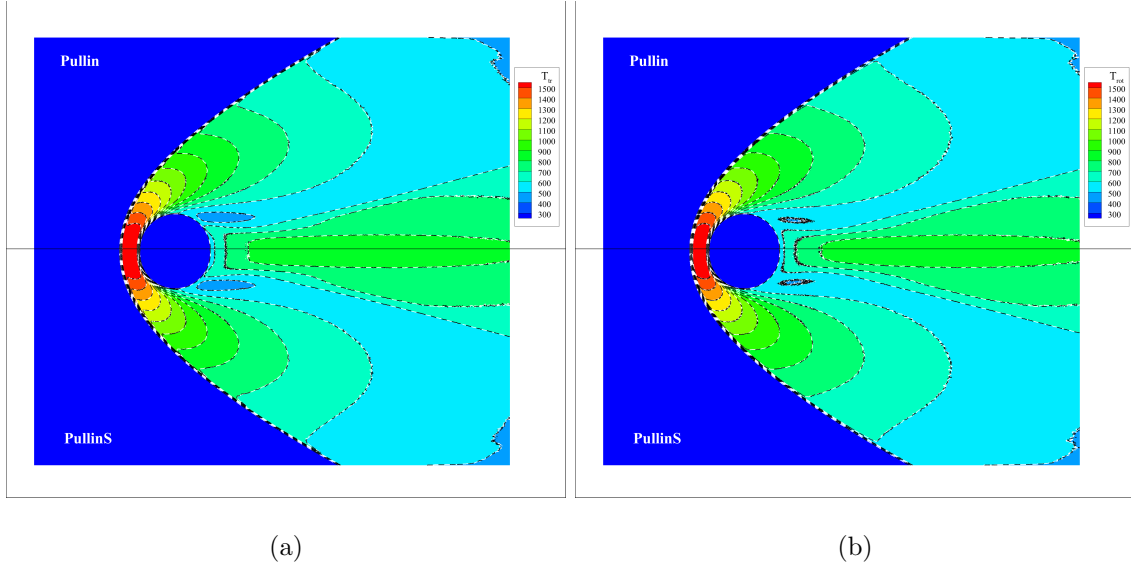


FIG. 7. Temperature contours of hypersonic cylinder flow at $\text{Ma} = 5$ and $\text{Kn} = 0.01$: (a) translational temperature; (b) rotational temperature. Upper solid line: Pullin model; lower solid line: simplified Pullin model; dashed line: BL model.

reflecting the strong nonequilibrium effects that dominate heat transfer in highly rarefied flows.

The computational times for all test cases are summarized in Table I. All computations are performed on the Computing Center in Xi'an using high-performance computing nodes, each equipped with dual Hygon 7285H 32C CPUs (2.5 GHz) and 256 GB memory. The non-linear variation of computational time with Knudsen number is primarily attributed to differences in the computational domain size and the ratio of grid spacing to the mean free path. In the near-continuum regime ($\text{Kn} = 0.01$), the Pullin model is 43.26% slower than the BL model, while its simplified variant is 32.62% slower, limiting the broad applicability of the Pullin model. With increasing rarefaction, the efficiency difference between the Pullin and BL models decreases, and under highly rarefied conditions ($\text{Kn} = 1$ and 10), their computational costs are comparable.

E. Hypersonic rarefied flow around an X38-like vehicle

To further evaluate the practical applicability of the Pullin model in aerospace flows, the hypersonic flow around the X38-like vehicle is investigated. A 1:16.7 scaled configuration

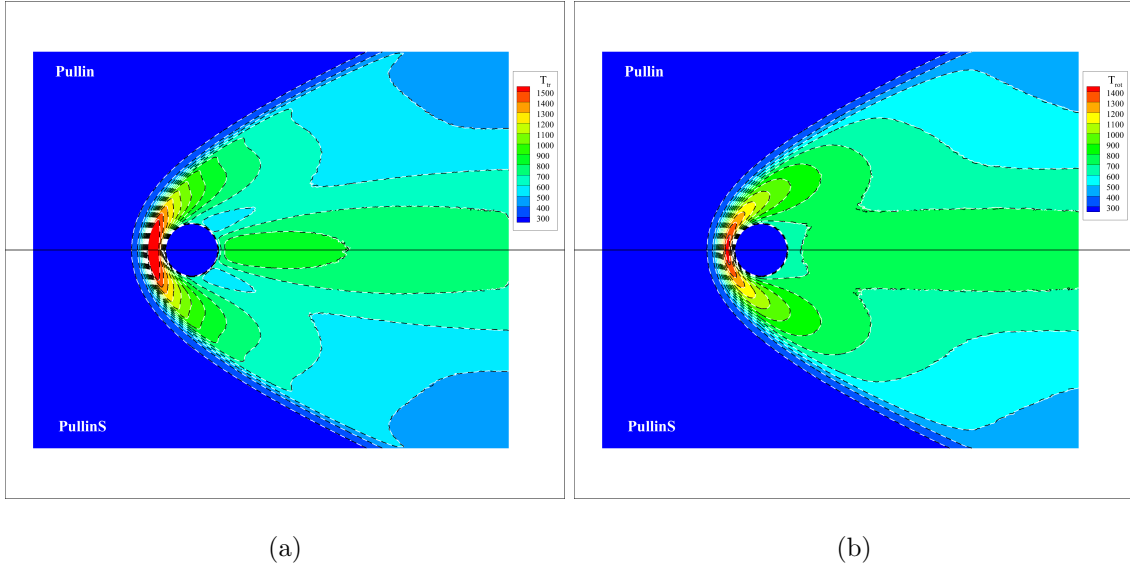


FIG. 8. Temperature contours of hypersonic cylinder flow at $\text{Ma} = 5$ and $\text{Kn} = 0.1$: (a) translational temperature; (b) rotational temperature. Upper solid line: Pullin model; lower solid line: simplified Pullin model; dashed line: BL model.

at four Knudsen numbers with $\text{Ma} = 8$, as well as the full-scale configuration at altitudes of 70-100 km with $\text{Ma} = 10$ and 20, were previously studied by Jiang et al.^{39,40} using the UGKS and DSMC methods. In the present study, the full-scale X38-like vehicle at altitudes of 90 km and 100 km is simulated using the DSMC method coupled with the Pullin model. A schematic of the X38-like vehicle is shown in Fig. 14, where the reference length L_{ref} is 4.67m and the reference area A_{ref} is 5.86m². The corresponding freestream parameters are summarized in Table IV. The working gas is air, with a reference diameter of 4.19Å and a viscosity index of 0.77 for the VHS model at 273 K. The freestream Mach number is set to $\text{Ma} = 10$, with an angle of attack of $\alpha = 20^\circ$, and both translational and rotational temperatures are initialized to $T_{tr} = T_{rot} = T_\infty$. The wall temperature is maintained at $T_{wall} = 300$ K under a fully diffusive boundary condition. The rotational collision number in the BL model is set to $Z_{BL} = 5$, while the corresponding parameter Z in the Pullin model is evaluated from Eq. (32). At an altitude of 100 km, the computational domain is discretized into 6,750,000 cells, with 20 simulated particles initialized per cell; whereas at 90 km, the domain is discretized into 125,000,000 cells, with 10 simulated particles per cell. All results are obtained by averaging over 40,000 time steps after reaching steady state.

Figures 15 and 16 present the rotational and translational temperature contours predicted

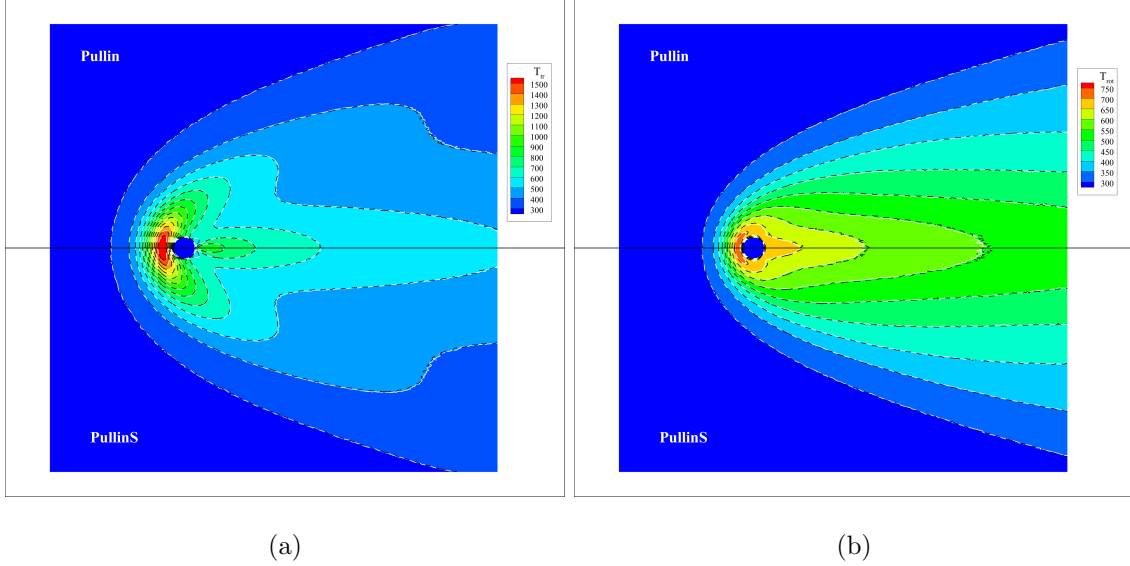


FIG. 9. Temperature contours of hypersonic cylinder flow at $\text{Ma} = 5$ and $\text{Kn} = 1.0$: (a) translational temperature; (b) rotational temperature. Upper solid line: Pullin model; lower solid line: simplified Pullin model; dashed line: BL model.

by the Pullin model at altitudes of 90 km and 100 km, respectively. At 90 km, the translational and rotational temperatures exhibit notable differences, indicating a significant degree of thermal nonequilibrium. As the flight altitude rises to 100 km, the maximum rotational temperature shifts away from the stagnation point, and the high-temperature region extends downstream, reflecting the strong nonequilibrium characteristics of the flow. Figures 17 and 18 compare the surface distributions of pressure, shear stress, and heat flux predicted by the three internal energy relaxation models at altitudes of 90 km and 100 km, respectively. The results obtained from the Pullin model and its simplified variant show good agreement with those predicted by the BL model. The overall aerodynamic coefficients of the X38-like vehicle are listed in Table V. The dimensionless coefficients are defined as

$$C_L = \frac{L}{0.5\rho_\infty U_\infty^2 A_{ref}}, \quad (40)$$

$$C_d = \frac{D}{0.5\rho_\infty U_\infty^2 A_{ref}},$$

where L and D denote the lift and drag forces, respectively. The Pullin model and its simplified variant show excellent agreement with BL results, with maximum relative errors of only 0.06% for the lift coefficient and 0.05% for the drag coefficient.

The computational times for all test cases are summarized in Table VI. All computations

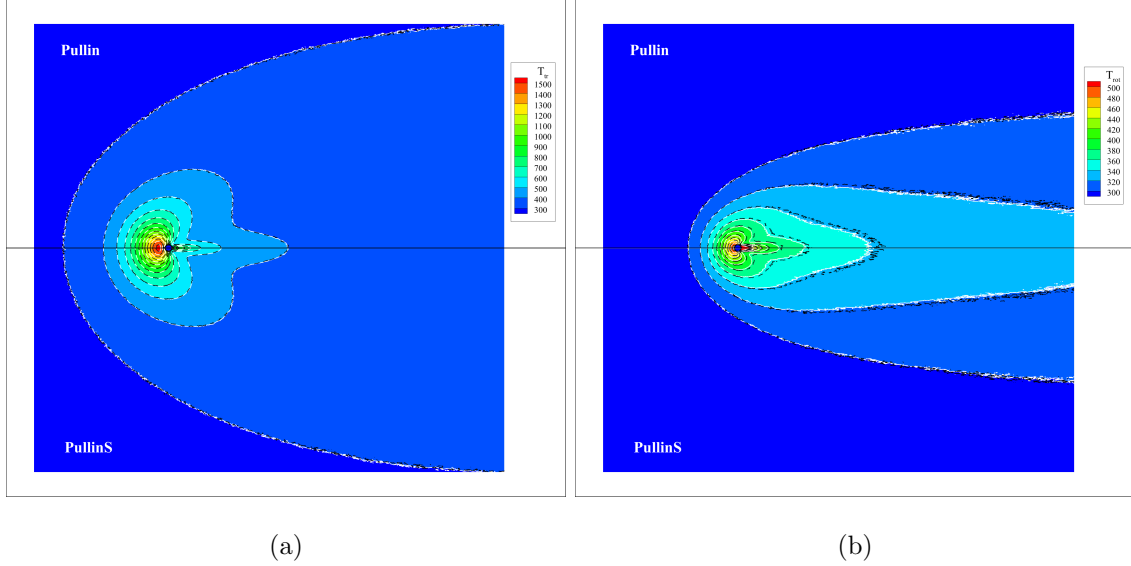


FIG. 10. Temperature contours of hypersonic cylinder flow at $\text{Ma} = 5$ and $\text{Kn} = 10$: (a) translational temperature; (b) rotational temperature. Upper solid line: Pullin model; lower solid line: simplified Pullin model; dashed line: BL model.

TABLE III. Comparison of the computational times required by different models for hypersonic flow past a cylinder.

Case	Models	No. of particles	N_{step}	CPU cores	Time(h)	CPU hours
$\text{Kn}=10^{-2}$	Pullin	36 932 194	80 000	60	10.1	606
	PullinS	36 936 927	80 000	60	9.35	561
	BL	36 935 474	80 000	60	7.05	423
$\text{Kn}=10^{-1}$	Pullin	6 767 054	80 000	30	1.39	41.7
	PullinS	6 768 071	80 000	30	1.28	38.4
	BL	6 766 777	80 000	30	1.07	32.1
$\text{Kn}=1$	Pullin	13 656 471	80 000	30	2.14	64.2
	PullinS	13 659 587	80 000	30	2.13	63.9
	BL	13 656 578	80 000	30	2.1	63
$\text{Kn}=10$	Pullin	45 656 769	80 000	60	4.76	285.6
	PullinS	45 656 113	80 000	60	4.76	285.6
	BL	45 654 716	80 000	60	4.73	283.8

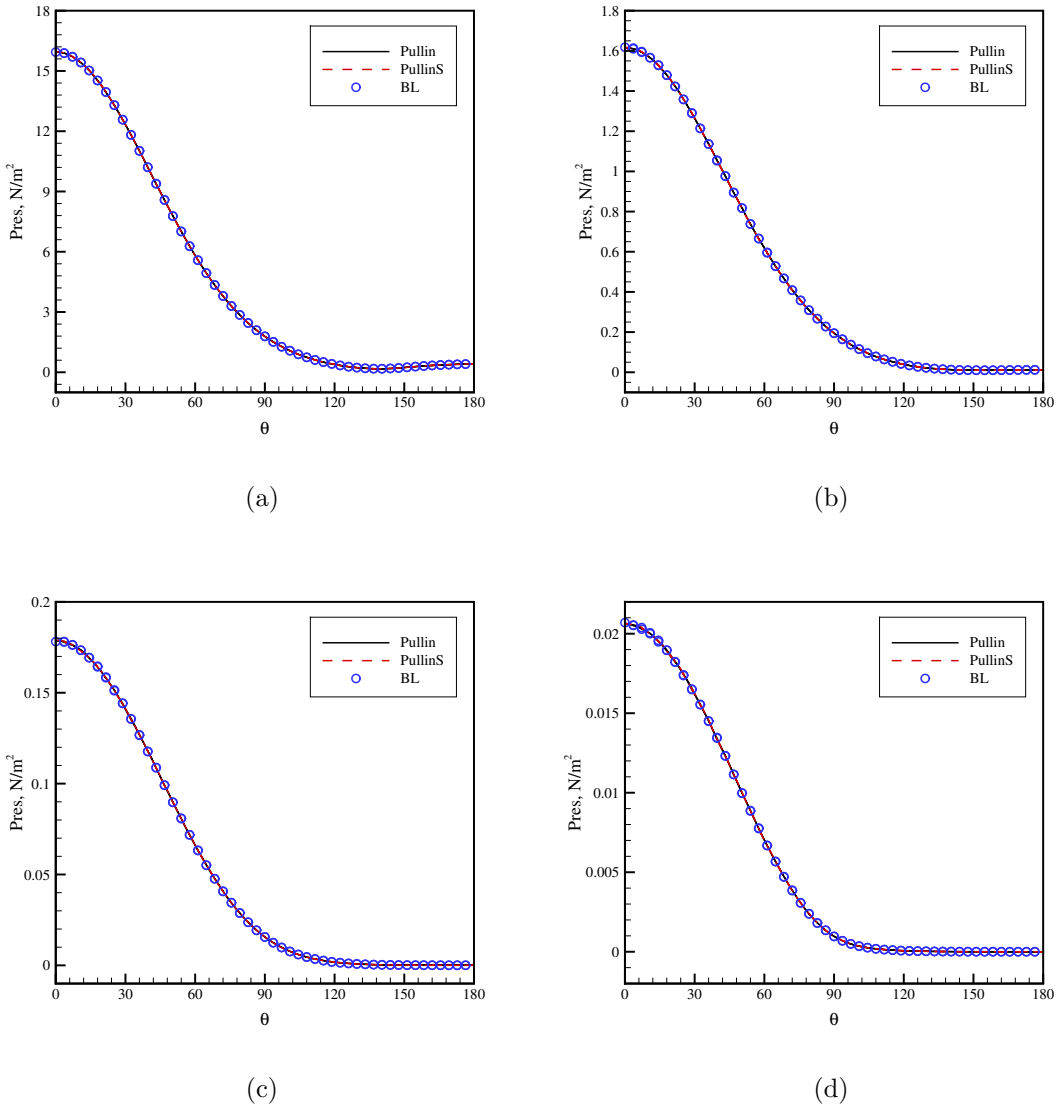


FIG. 11. Surface pressure results of hypersonic cylinder flow at $\text{Ma} = 5$: (a) $\text{Kn} = 0.01$, (b) $\text{Kn} = 0.1$, (c) $\text{Kn} = 1.0$, (d) $\text{Kn} = 10.0$. Solid line: Pullin model; dashed line: simplified Pullin model; circles: BL model.

TABLE IV. Freestream conditions for hypersonic flow around an X38-like vehicle at altitudes of 90 and 100 km.

Altitude(km)	Gas	Ma	$n_{\infty}(m^{-3})$	$T_{\infty}(\text{K})$	$T_{wall}(\text{K})$	α	$R(\text{J}/(\text{kg} \cdot \text{K}))$	Z_{BL}
90	Air	10	7.116×10^{19}	186.867	300	20°	286.71	5.0
100	Air	10	1.189×10^{19}	195.081	300	20°	286.71	5.0

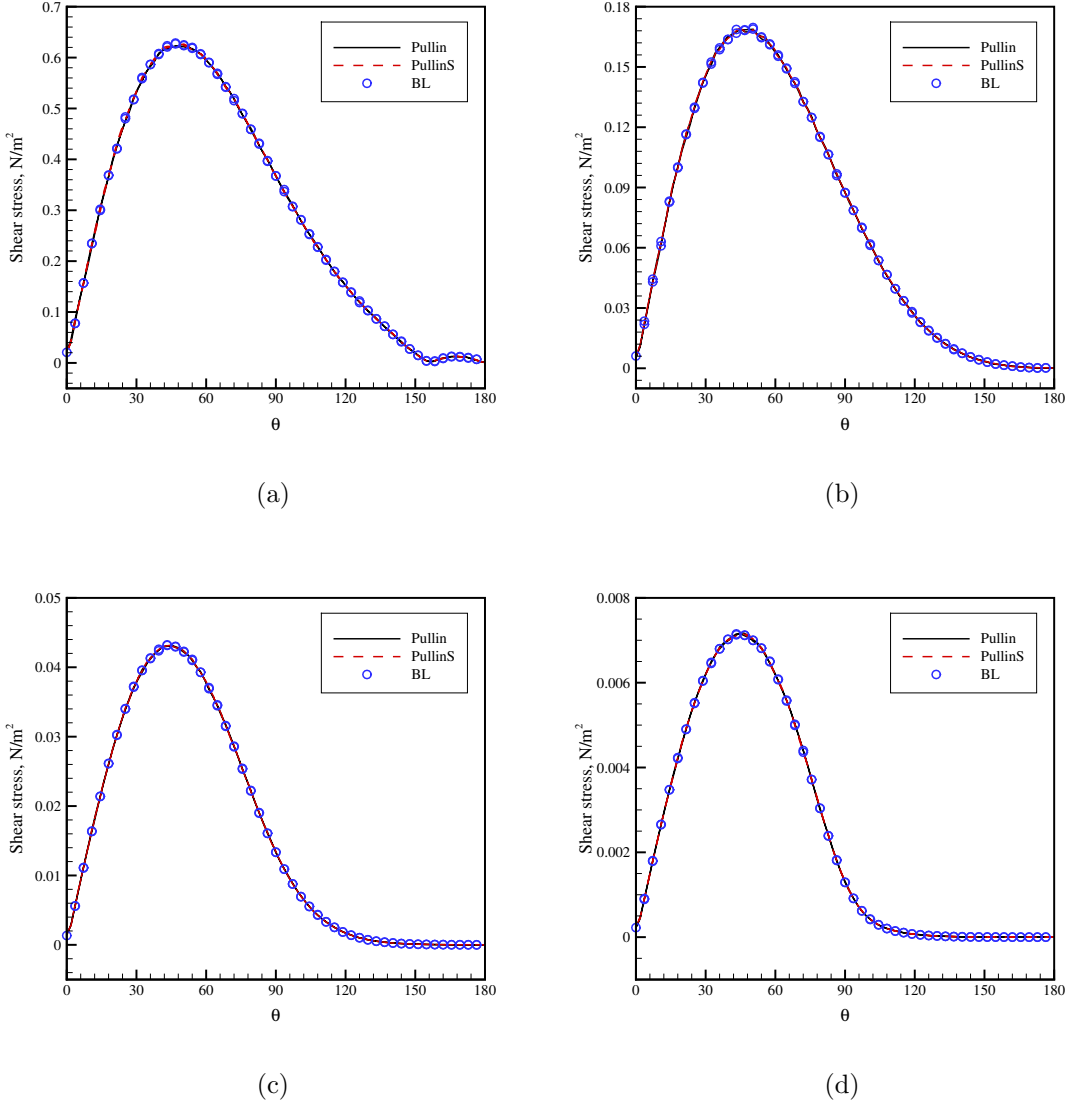


FIG. 12. Surface shear stress results of hypersonic cylinder flow at $Ma = 5$: (a) $Kn = 0.01$, (b) $Kn = 0.1$, (c) $Kn = 1.0$, (d) $Kn = 10.0$. Solid line: Pullin model; dashed line: simplified Pullin model; circles: BL model.

are performed on the Computing Center in Xi'an using high-performance computing nodes, each equipped with dual Hygon 7285H 32C CPUs (2.5 GHz) and 256 GB memory. At an altitude of 90 km, the Pullin model is approximately 20.81% slower than the BL model, while its simplified variant is 13.4% slower. As the flight altitude increases to 100 km, the differences are reduced to 8.36% and 4.1%, respectively. For simulations above 100 km, the choice of model has a negligible impact on computational efficiency.

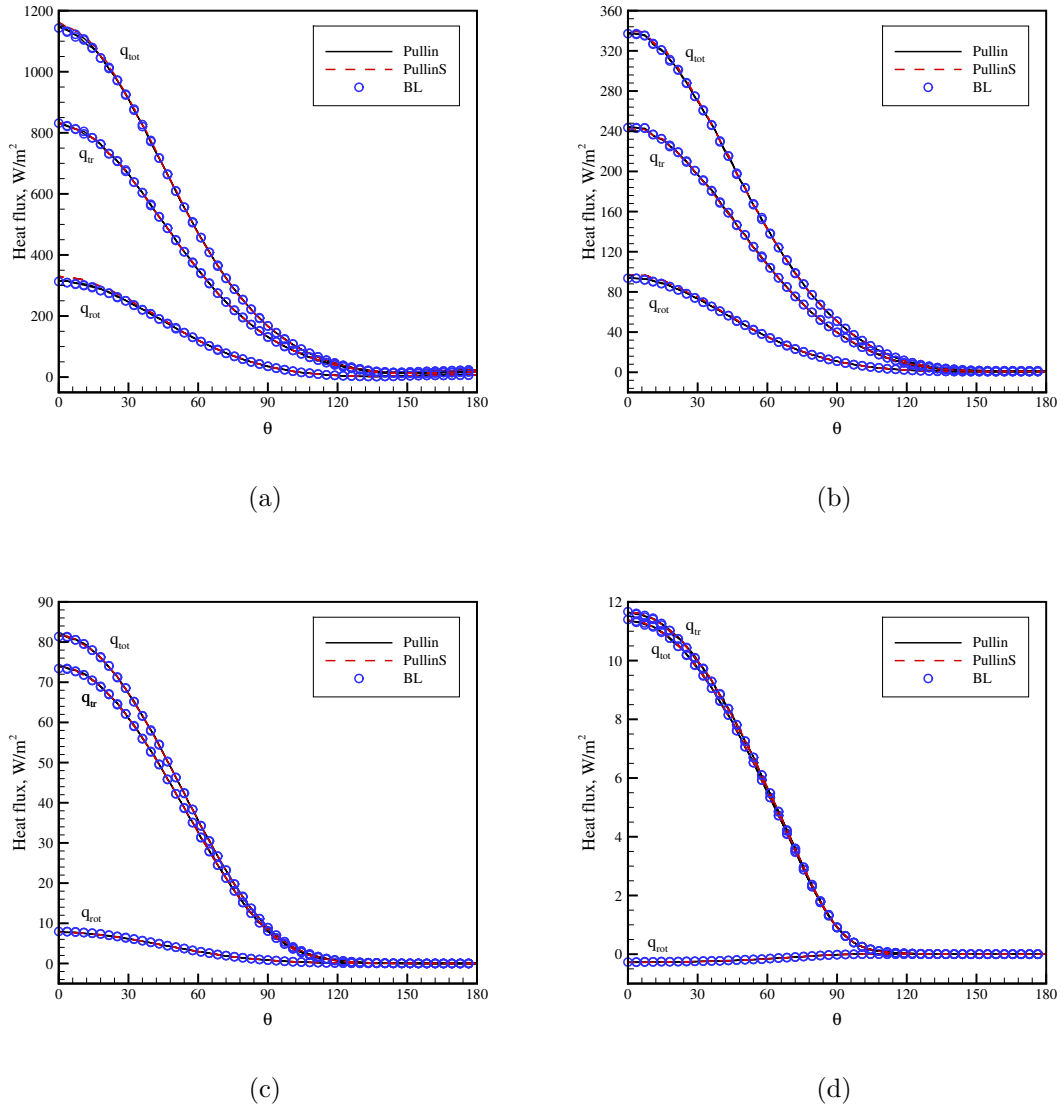


FIG. 13. Surface heat flux results of hypersonic cylinder flow at $\text{Ma} = 5$: (a) $\text{Kn} = 0.01$, (b) $\text{Kn} = 0.1$, (c) $\text{Kn} = 1.0$, (d) $\text{Kn} = 10.0$. Solid line: Pullin model; dashed line: simplified Pullin model; circles: BL model.

TABLE V. Comparison of aerodynamic coefficients of the X38-like vehicle at Mach 10.

Altitude(km)	Coefficients	BL	Pullin	Relative error	PullinS	Relative error
90	C_L	0.3142	0.3142	-	0.3140	-0.06%
	C_d	0.2708	0.2708	-	0.2709	-0.04%
100	C_L	0.39	0.3902	0.05%	0.3901	0.03%
	C_d	0.5140	0.5140	-	0.5142	0.04%

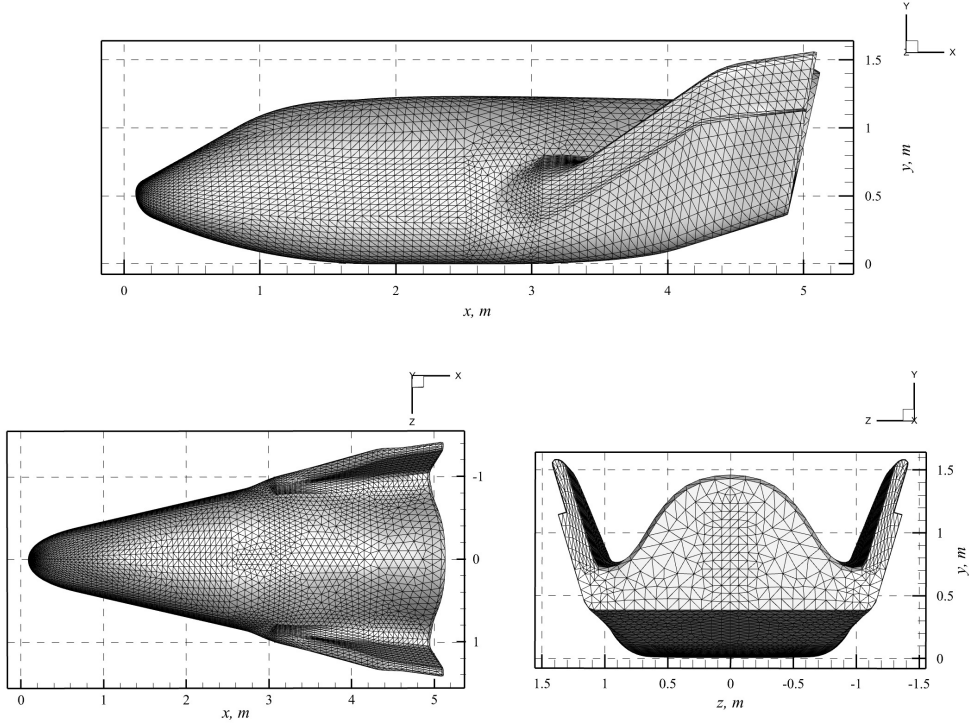


FIG. 14. Sketch of the X38-like vehicle (17,414 triangles in the surface mesh).

TABLE VI. Comparison of the computational time required for different models for the hypersonic flow around X38-like vehicle.

Altitude(km)	Models	No. of particles	N_{step}	CPU cores	Time(h)	CPU hours
90	Pullin	1 270 009 678	80 000	300	59.69	17907
	PullinS	1 270 009 737	80 000	300	56.03	16809
	BL	1 269 992 103	80 000	300	49.41	14823
100	Pullin	136 497 915	80 000	150	6.61	991.5
	PullinS	136 495 963	80 000	150	6.35	952.5
	BL	136 489 077	80 000	150	6.1	915

V. CONCLUSIONS

In this work, a new parameterization of the Pullin model for VHS molecules has been proposed, establishing a direct link between the partition parameter and the rotational collision number. Compared with the widely used BL model, the Pullin framework—derived from gas kinetic theory—offers improved physical fidelity by enabling rotational relaxation

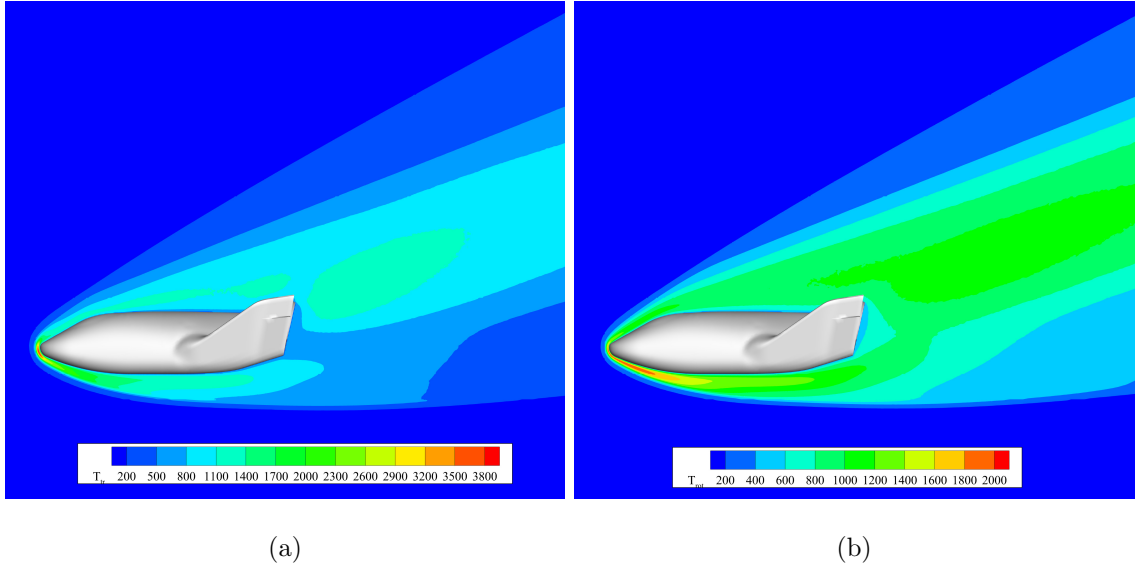


FIG. 15. Temperature contour results for hypersonic flow around an X38-like vehicle at 90 km altitude: (a) translational temperature, (b) rotational temperature.

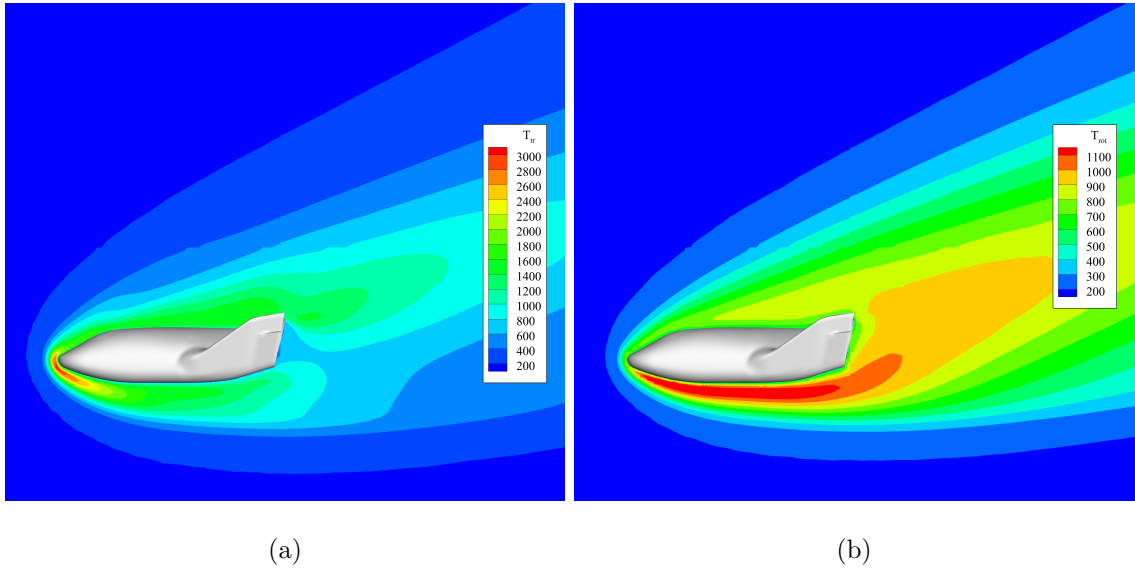


FIG. 16. Temperature contour results for hypersonic flow around an X38-like vehicle at 100 km altitude: (a) translational temperature, (b) rotational temperature.

of internal energy in all simulated particles. With the proposed parameterization, both the full and simplified Pullin models have been successfully extended to diatomic VHS gases. Since the energy exchange requires sampling only three or five Beta-distributed variates, these models can be implemented easily within the DSMC framework.

The accuracy and efficiency of the Pullin model and its simplified variant have been

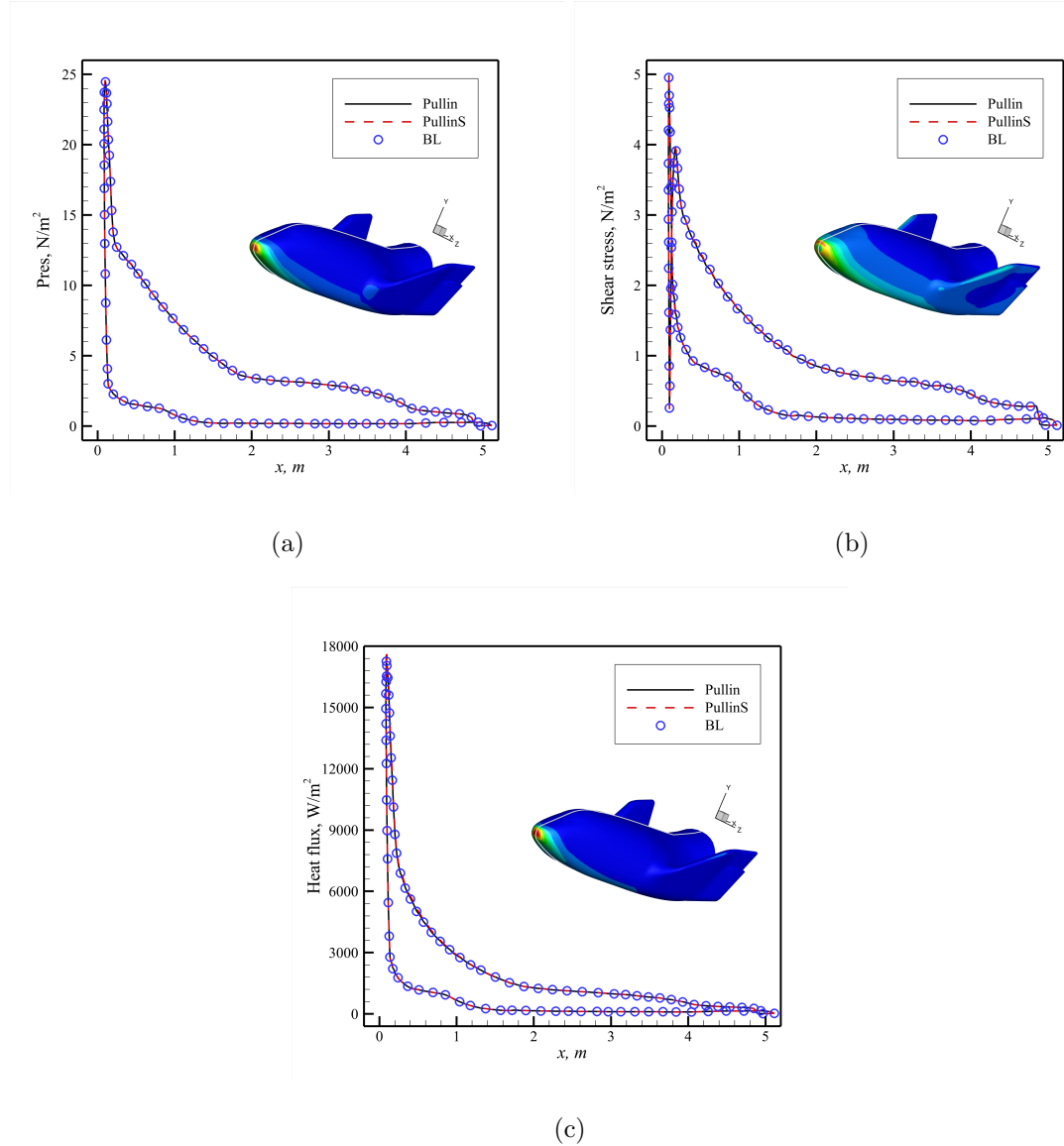


FIG. 17. Surface results for hypersonic flow around an X38-like vehicle at 90 km altitude: (a) pressure, (b) shear stress, (c) heat flux. Solid line: Pullin model; dashed line: simplified Pullin model; circles: BL model.

validated through a series of numerical test cases—including zero-dimensional rotational relaxation of nitrogen, one-dimensional planar Couette flow and normal shock wave, two-dimensional hypersonic flow past a cylinder, and three-dimensional hypersonic flow around an X38-like vehicle—and systematically compared with the BL model. In all cases, both the full and simplified Pullin models show excellent agreement with reference solutions from theory, experiments, and the BL model. In the near-continuum regimes (Knudsen number Kn

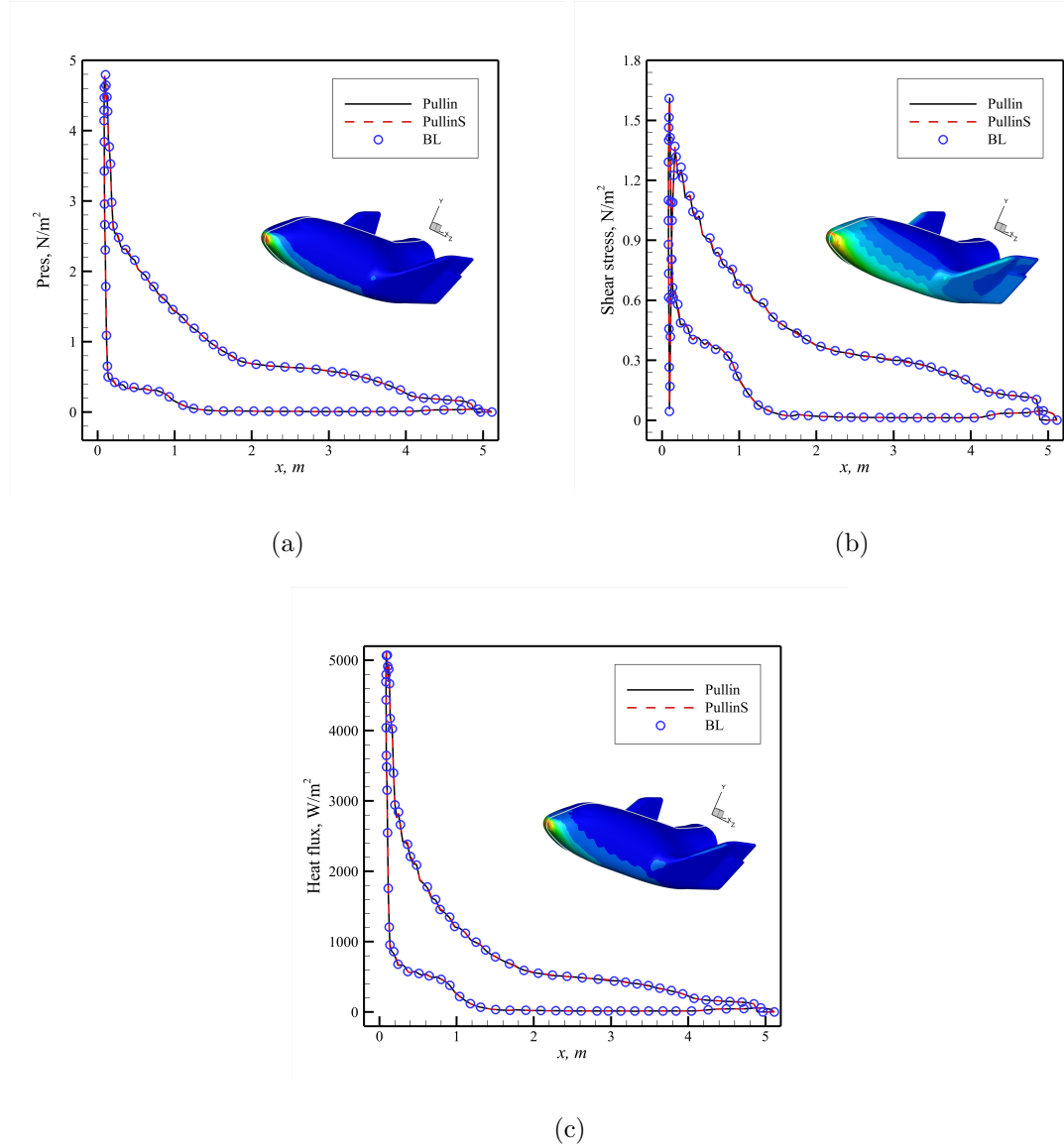


FIG. 18. Surface results for hypersonic flow around an X38-like vehicle at 100 km altitude: (a) pressure, (b) shear stress, (c) heat flux. Solid line: Pullin model; dashed line: simplified Pullin model; circles: BL model.

$= 0.01$, or altitudes below 90 km), the Pullin model is approximately 20 \sim 40% slower than the BL model due to the additional computational cost of sampling Beta-distributed variates. However, in the highly rarefied flow regimes of DSMC simulations (Knudsen number greater than 1, or altitudes above 100 km), the simplified Pullin model exhibits performance comparable to the BL model.

Overall, the Pullin model and its simplified variant offer a robust and practical alter-

native to the BL model within the DSMC framework, providing improved physical fidelity in representing rotational energy relaxation with only a modest computational cost. Their demonstrated accuracy across a wide range of test cases underscores their suitability for hypersonic aerothermodynamic applications. Future work will extend the simplified Pullin model by incorporating vibrational relaxation, thereby enhancing its applicability to high-enthalpy nonequilibrium flows.

ACKNOWLEDGEMENTS

The authors thank Mr. Rui Zhang and Mr. Jianfeng Chen for their valuable discussions on kinetic models of internal energy relaxation. This work was financially supported by the National Natural Science Foundation of China (Grants 12172301), and the Program of Introducing Talents of Discipline to Universities (111 Project of China, Grant B17037).

DATA AVAILABILITY

The data that support the findings of this study are available from the corresponding author upon reasonable request.

REFERENCES

¹W. Zhang, Z. Zhang, X. Wang, and T. Su, “A review of the mathematical modeling of equilibrium and nonequilibrium hypersonic flows,” *Advances in Aerodynamics* **4**, 38 (2022).

²J. D. Anderson, *Hypersonic and high temperature gas dynamics* (AIAA, 1989).

³I. D. Boyd and T. E. Schwartzentruber, *Nonequilibrium gas dynamics and molecular simulation*, Vol. 42 (Cambridge University Press, 2017).

⁴M. Schouler, Y. Prévereaud, and L. Mieussens, “Survey of flight and numerical data of hypersonic rarefied flows encountered in earth orbit and atmospheric reentry,” *Progress in Aerospace Sciences* **118**, 100638 (2020).

⁵S. Liu, P. Yu, K. Xu, and C. Zhong, “Unified gas-kinetic scheme for diatomic molecular simulations in all flow regimes,” *Journal of Computational Physics* **259**, 96–113 (2014).

⁶W. Hu, Z. Li, A. Peng, and X. Jiang, “A gas-kinetic unified algorithm for non-equilibrium polyatomic gas flows covering various flow regimes,” *Communications in Computational Physics* **30**, 144–189 (2021).

⁷Q. Zhang, C. Zhuo, J. Mu, C. Zhong, and S. Liu, “A multiscale discrete velocity method for diatomic molecular gas,” *Physics of Fluids* **35** (2023).

⁸G. A. Bird, *Molecular gas dynamics and the direct simulation of gas flows* (Oxford university press, 1994).

⁹M. Pfeiffer, “Extending the particle ellipsoidal statistical Bhatnagar-Gross-Krook method to diatomic molecules including quantized vibrational energies,” *Physics of Fluids* **30** (2018).

¹⁰X. Xu, Y. Chen, C. Liu, Z. Li, and K. Xu, “Unified gas-kinetic wave-particle methods V: Diatomic molecular flow,” *Journal of Computational Physics* **442**, 110496 (2021).

¹¹F. Fei, Y. Hu, and P. Jenny, “A unified stochastic particle method based on the Bhatnagar-Gross-Krook model for polyatomic gases and its combination with DSMC,” *Journal of Computational Physics* **471**, 111640 (2022).

¹²G. A. Bird, *The DSMC method* (CreateSpace Independent Publishing Platform, 2013).

¹³V. Kosyanchuk and A. Yakunchikov, “A detailed multiscale study of rotational-translational relaxation process of diatomic molecules,” *Physics of Fluids* **33** (2021).

¹⁴Z. Eckert and M. A. Gallis, “Enforcing detailed balance in the Borgnakke–Larsen redistribution method with temperature dependent relaxation models,” *Physics of Fluids* **34** (2022).

¹⁵S. Trivedi, J. S. Salinas, J. K. Harvey, A. Y. Poludnenko, and J. H. Chen, “Simulations of hydrogen-air detonations using Direct Simulation Monte Carlo,” *Combustion and Flame* **279**, 114333 (2025).

¹⁶G. Gokul and G. Malaikannan, “Insights into chemical kinetics of hybrid chemical reaction models in hypersonic rarefied flow,” *Physics of Fluids* **36** (2024).

¹⁷M. Fang, Z. Li, Z. Li, J. Liang, and Y. Zhang, “DSMC modeling of rarefied ionization reactions and applications to hypervelocity spacecraft reentry flows,” *Advances in Aerodynamics* **2**, 7 (2020).

¹⁸C. Borgnakke and P. S. Larsen, “Statistical collision model for Monte Carlo simulation of polyatomic gas mixture,” *Journal of computational Physics* **18**, 405–420 (1975).

¹⁹D. Pullin, “Kinetic models for polyatomic molecules with phenomenological energy exchange,” *Physics of Fluids* **21**, 209–216 (1978).

²⁰A. Erofeev, “Numerical investigation of the effect of rotational relaxation rate on the nitrogen shock wave structure,” *Fluid dynamics* **30**, 621–628 (1995).

²¹P. Prasanth, J. K. Kakkassery, and R. Vijayakumar, “A variable hard sphere-based phenomenological inelastic collision model for rarefied gas flow simulations by the direct simulation Monte Carlo method,” *Fluid Dynamics Research* **44**, 025503 (2012).

²²M. N. Macrossan, “Rotation-translation collision model for DSMC with restricted energy exchange,” *International Journal for Numerical Methods in Fluids* **93**, 3254–3263 (2021).

²³X. Lu and Z. Ye, “A universal method of redistributing relaxation energies in inelastic molecular collisions,” *Physics of Fluids* **34** (2022).

²⁴B. L. Haas, D. B. Hash, G. A. Bird, F. E. Lumpkin, and H. Hassan, “Rates of thermal relaxation in direct simulation Monte Carlo methods,” *Physics of Fluids* **6**, 2191–2201 (1994).

²⁵I. D. Boyd, “Temperature dependence of rotational relaxation in shock waves of nitrogen,” *Journal of Fluid Mechanics* **246**, 343–360 (1993).

²⁶P. Vijayakumar, Q. Sun, and I. D. Boyd, “Vibrational–translational energy exchange models for the direct simulation Monte Carlo method,” *Physics of Fluids* **11**, 2117–2126 (1999).

²⁷S. Liu, N. Ding, M. Fang, H. Jin, R. Zhang, C. Zhuo, and C. Zhong, “The near-continuum mechanism for extended Boltzmann theory: the non-equilibrium relaxation,” (2026), arXiv:2602.05775.

²⁸G. A. Bird, “Direct simulation and the Boltzmann equation,” *Physics of Fluids* **13**, 2676–2681 (1970).

²⁹G. A. Bird, *The DSMC method* (CreateSpace Independent Publishing Platform, 2013).

³⁰J. Parker, “Rotational and vibrational relaxation in diatomic gases,” *The Physics of Fluids* **2**, 449–462 (1959).

³¹E. Carnevale, C. Carey, and G. Larson, “Ultrasonic determination of rotational collision numbers and vibrational relaxation times of polyatomic gases at high temperatures,” *The Journal of Chemical Physics* **47**, 2829–2835 (1967).

³²M. Jöhnk, “Erzeugung von betaverteilten und gammaverteilten zufallszahlen,” *Metrika* **8**, 5–15 (1964).

³³R. C. Cheng, “Generating beta variates with nonintegral shape parameters,” *Communications of the ACM* **21**, 317–322 (1978).

³⁴S. J. Plimpton, S. G. Moore, A. Borner, A. K. Stagg, T. P. Koehler, J. R. Torczynski, and M. A. Gallis, “Direct simulation Monte Carlo on petaflop supercomputers and beyond,” *Physics of Fluids* **31** (2019).

³⁵L. Wu, C. White, T. J. Scanlon, J. M. Reese, and Y. Zhang, “A kinetic model of the Boltzmann equation for non-vibrating polyatomic gases,” *Journal of Fluid Mechanics* **763**, 24–50 (2015).

³⁶F. Robben and L. Talbot, “Experimental study of the rotational distribution function of nitrogen in a shock wave,” *The Physics of Fluids* **9**, 653–662 (1966).

³⁷H. Alsmeyer, “Density profiles in argon and nitrogen shock waves measured by the absorption of an electron beam,” *Journal of Fluid Mechanics* **74**, 497–513 (1976).

³⁸I. D. Boyd, “Rotational–translational energy transfer in rarefied nonequilibrium flows,” *Physics of Fluids A: Fluid Dynamics* **2**, 447–452 (1990).

³⁹D. Jiang, M. Mao, J. Li, and X. Deng, “An implicit parallel UGKS solver for flows covering various regimes,” *Advances in Aerodynamics* **1**, 8 (2019).

⁴⁰D. Jiang, P. Wang, J. Li, and M. Mao, “Nonlinear modeling study of aerodynamic characteristics of an X38-like vehicle at strong viscous interaction regions,” *Entropy* **24**, 836 (2022).